International Journal of Entomology Research
www.entomologyjournals.com
ISSN: 2455-4758
Received: 05-08-2026, Accepted: 04-09-2026, Published: 19-09-2026
Volume 11, Issue 3, 2026, Page No. 644-663

Eco-friendly fabrication of silver nanoparticles using *Acheta domesticus* (House Cricket) biomass: characterization and broad-spectrum antibacterial efficacy against Multidrug-Resistant Clinical Isolates

Dr. Jay Prakash Singh[1], Chaitali Mahesh Kulkarni[2], Dr. Subhashish Tripathy[3], Dr. Hridaya Shankar Chaurasiya[4], Dipika[5]

[1] Associate Professor, BMS College of Pharmacy, Amethi, Uttar Pradesh, India
[2] Department of Pharmaceutics, P.E. Society's Modern College of Pharmacy nigdi Yamunangar Pune, Affiliated to Savitribai Phule Pune University, Maharashtra, India
[3] Professor, B.M.S. College of Pharmacy, Tiloi, Amethi, Uttar Pradesh, India
[4] Principal, Jyotiraditya Institute of Pharmacy, JD Shiksha Gram, Pratapgarh, Uttar Pradesh, India
[5] Assistant Professor, BMS College of Pharmacy, Nasratpur, Tiloi, Amethi, Uttar Pradesh, India
Corresponding Author: Dr. Jay Prakash Singh
DOI: https://doi.org/10.66856/ijer.2026.11.3.11333

Abstract

Background: The global rise of multidrug-resistant (MDR) clinical pathogens has created an urgent need for novel antibacterial agents. Green synthesis of silver nanoparticles (Ag NPs) using biological extracts offers an eco-friendly, cost-effective alternative to conventional chemical methods. Insects represent an underexplored but promising biogenic resource due to their high protein and chitin content, low environmental footprint, and established farming infrastructure. The house cricket (*Acheta domesticus*) is widely farmed as a sustainable protein source but has not been systematically investigated for nanoparticle synthesis.

Objective: To synthesize silver nanoparticles using aqueous extract of house cricket (*Acheta domesticus*), optimize the synthesis parameters, comprehensively characterize the nanoparticles, and evaluate their antibacterial activity against a panel of clinically relevant multidrug-resistant pathogens.

Methods: Aqueous cricket extract was prepared by boiling crushed adult crickets in deionized water. Ag NPs were synthesized by adding 1 mM silver nitrate to the extract under varying conditions (extract: Ag NO_3 ratio 1:1 to 1:20, pH 3–11, temperature 25–100°C, time 0–120 minutes) to determine optimal parameters. Characterization was performed using UV-Vis spectroscopy, Fourier transform infrared (FTIR) spectroscopy, X-ray diffraction (XRD), dynamic light scattering (DLS), zeta potential analysis, scanning electron microscopy (SEM) with energy-dispersive X-ray spectroscopy (EDX), and transmission electron microscopy (TEM). Antibacterial activity was tested against five clinical MDR isolates: methicillin-resistant *Staphylococcus aureus* (MRSA), extended-spectrum beta-lactamase (ESBL)-producing *Escherichia coli*, carbapenem-resistant *Klebsiella pneumoniae* (CR-KP), multidrug-resistant *Pseudomonas aeruginosa* (MDR-PA), and vancomycin-resistant *Enterococcus faecalis* (VRE). Activity was assessed by agar well diffusion (zone of inhibition, ZOI) and broth microdilution (minimum inhibitory concentration, MIC, minimum bactericidal concentration, MBC).

Results: Optimal synthesis conditions were established as 1:5 extract: $AgNO_3$ ratio, pH 8, 60°C, and 60 minutes, yielding a characteristic dark brown color indicative of AgNP formation. UV-Vis spectroscopy confirmed the surface plasmon resonance (SPR) peak at 428 nm. FTIR revealed amide I (1645 → 1628 cm^{-1}) and amide II (1538 → 1520 cm^{-1}) shifts, indicating protein chemisorption as the capping mechanism. XRD confirmed a face-centered cubic crystalline structure with an average crystallite size of 23 nm. DLS showed a Z-average hydrodynamic diameter of 68.4 ± 4.2 nm (polydispersity index 0.214), while TEM revealed predominantly spherical nanoparticles (82%) with a mean primary size of 28.3 ± 6.7 nm (range 15–45 nm). Zeta potential was -32.5 ± 2.8 mV, indicating good colloidal stability. EDX confirmed silver as the major elemental component (73.2 wt%), with carbon, oxygen, and nitrogen from the capping layer.

The AgNPs exhibited concentration-dependent antibacterial activity against all five MDR pathogens. The ZOI at 200 µg/mL ranged from 15.8 mm (VRE) to 21.5 mm (ESBL *E. coli*). MIC values were 8 µg/mL for ESBL *E. coli*, 16 µg/mL for MRSA, and 32 µg/mL for CR-KP, MDR-PA, and VRE. MBC values were twice the MIC for all strains (MBC/MIC = 2), confirming bactericidal activity. The cricket extract alone showed no antibacterial activity, confirming that the observed effects are attributable to the nanoparticles.

Conclusion: *Acheta domesticus* extract is an effective, sustainable reducing and capping agent for the green synthesis of stable, crystalline silver nanoparticles. The cricket-synthesized AgNPs exhibit potent, dose-dependent, bactericidal activity against clinically relevant multidrug-resistant pathogens, including strains resistant to multiple conventional antibiotics. These findings support the potential application of cricket-synthesized AgNPs in topical antimicrobial formulations, wound dressings, and medical device coatings. Further studies are warranted to assess *in vivo* efficacy, safety, and scalability.

Keywords: Green synthesis, Silver nanoparticles, Acheta domesticus, House cricket, Antibacterial activity, Multidrug-resistant clinical pathogens, Methicillin-resistant Staphylococcus aureus (MRSA), Extended-spectrum beta-lactamase (ESBL)-

producing Escherichia coli, Carbapenem-resistant Klebsiella pneumoniae (CR-KP), Vancomycin-resistant Enterococcus faecalis (VRE), Protein capping, Chitin, Surface plasmon resonance, Bactericidal, Green chemistry, Nanobiotechnology

Introduction

The Global Crisis of Antibiotic Resistance

The discovery and widespread deployment of antibiotics in the mid-20th century represented one of the greatest triumphs of modern medicine. Infections that had been death sentences for millennia—pneumonia, puerperal fever, wound infections, tuberculosis—became treatable, even curable. Surgical procedures, organ transplants, and cancer chemotherapy, all of which rely on the ability to prevent and treat bacterial infections, became routine. However, this golden age is rapidly drawing to a close. The World Health Organization has declared antimicrobial resistance (AMR) one of the top ten global public health threats facing humanity, warning that we are entering a "post-antibiotic era" in which common infections and minor injuries may once again kill [1].

The scale of the crisis is staggering. In 2019 alone, an estimated 4.95 million deaths were associated with bacterial AMR, with 1.27 million deaths directly attributable to resistant infections. This makes AMR a leading cause of death globally, surpassing HIV/AIDS and malaria combined. The economic burden is equally severe, with the World Bank projecting that unchecked AMR could cause $1 trillion to $3.4 trillion in annual GDP losses by 2030, pushing an additional 24 million people into extreme poverty.

Clinical pathogens of particular concern have become endemic in hospital settings worldwide. Methicillin-resistant *Staphylococcus aureus* (MRSA) alone causes over 120,000 deaths annually and is associated with significantly longer hospital stays and higher mortality than susceptible strains. Extended-spectrum beta-lactamase (ESBL)-producing *Escherichia coli* and *Klebsiella pneumoniae* have rendered many frontline cephalosporins useless.

Fig 1: Morphological close-up of Blaptica dubia *(Dubia roach).* The image illustrates the head region, compound eyes, antennae, and mouthparts used for sensory perception and feeding. This specimen serves as the biological source of hemolymph utilized for in-vitro anticancer and biochemical analyses.

Carbapenem-resistant *Pseudomonas aeruginosa* is a particular threat in intensive care units and among immunocompromised patients, with mortality rates exceeding 50% in some studies. Vancomycin-resistant *Enterococcus faecalis* (VRE) complicates the management of urinary tract, bloodstream, and wound infections, especially in hospitalized patients.

The pipeline for new antibiotics has remained alarmingly dry for decades. Between 2017 and 2021, only 12 new antibiotics received regulatory approval, and most are derivatives of existing classes with predictable cross-resistance. The economic model for antibiotic development is fundamentally broken: antibiotics are used for short durations, are priced low (often below their true value), and resistance inevitably erodes their market lifespan. Consequently, most major pharmaceutical companies have abandoned antibiotic research entirely. The few remaining small biotechnology companies developing novel antibiotics face high failure rates and precarious finances [2].

This therapeutic void has driven researchers to explore alternative strategies outside the traditional antibiotic paradigm. Antimicrobial peptides derived from frogs, insects, and humans show promise but face challenges with stability and toxicity. Phage therapy—using viruses that specifically infect bacteria—has seen a resurgence but remains highly personalized and logistically complex. Fecal microbiota transplantation can treat recurrent *Clostridioides difficile* infections but has limited applicability to other pathogens.

Among the most promising alternative approaches is the use of metallic nanoparticles, particularly silver nanoparticles (AgNPs), as broad-spectrum antibacterial agents. Unlike conventional antibiotics that typically target a single bacterial protein or pathway, nanoparticles can attack multiple cellular components simultaneously, theoretically making it more difficult for bacteria to develop resistance. This multi-target mechanism, combined with the unique size-dependent properties of nanomaterials, positions AgNPs as a potentially transformative platform for combating drug-resistant infections.

Silver Nanoparticles: Mechanisms and Advantages

Silver has been recognized for its antimicrobial properties since ancient times. The Phoenicians, Greeks, Romans, and Egyptians all used silver vessels to preserve water and other liquids. In the 19th century, silver nitrate was used to prevent gonococcal ophthalmia neonatorum in newborns. The advent of antibiotics in the 20th century displaced silver from routine clinical use, but the rise of antibiotic resistance has revived interest in this ancient antimicrobial.

The advent of nanotechnology has dramatically enhanced silver's antibacterial potential. By reducing silver to the nanoscale (1–100 nm), the surface-area-to-volume ratio increases exponentially, maximizing contact with bacterial cells. A single gram of 10 nm silver nanoparticles has a surface area of approximately 50 square meters, compared to only 0.01 square meters for a gram of bulk silver. This

enormous surface area enhances both the release of antimicrobial silver ions and direct nanoparticle-bacteria interactions.

The antibacterial mechanisms of AgNPs are multiple, synergistic, and not fully understood. The current consensus recognizes several interconnected pathways:

Membrane disruption: AgNPs adhere to bacterial cell surfaces through electrostatic and hydrophobic interactions. Once bound, they can disrupt membrane integrity by (i) forming physical pores, (ii) altering membrane fluidity and permeability, (iii) interfering with electron transport chains, and (iv) causing lipid peroxidation. Gram-negative bacteria have an additional outer membrane containing lipopolysaccharide (LPS), which presents an initial barrier, but porin channels may actually facilitate AgNP entry.

Reactive oxygen species (ROS) generation: AgNPs catalyze the production of ROS including superoxide ($O_2^{\bullet -}$), hydrogen peroxide (H_2O_2), and the highly destructive hydroxyl radical (•OH). ROS cause widespread oxidative damage to bacterial components: DNA strand breaks and base modifications, protein carbonylation and aggregation, and lipid peroxidation leading to membrane breakdown. The resulting oxidative stress overwhelms bacterial antioxidant defences, leading to cell death.

Metal ion release and toxicity: AgNPs slowly release Ag^+ ions, which are highly toxic to bacteria. Silver ions bind strongly to thiol (-SH) groups in proteins, inactivating essential enzymes including those involved in respiration (NADH dehydrogenase), metabolism, and DNA replication. Silver ions also displace other metal cofactors from metalloenzymes, disrupting their catalytic function [3].

Intracellular penetration and DNA damage: Smaller AgNPs (particularly those under 30 nm) can penetrate bacterial cells, either through damaged membranes or via porin channels. Inside the cytoplasm, AgNPs and released Ag^+ ions can directly bind to DNA, causing condensation, strand breaks, and inhibition of replication and transcription. Ribosomal dysfunction and inhibition of protein synthesis have also been reported.

This multi-target mechanism is a critical advantage. Whereas a bacterium might acquire a single mutation to evade a conventional antibiotic (e.g., altering the target binding site or acquiring a drug-degrading enzyme), evolving resistance to a multi-target agent is statistically far less likely. Studies have shown that bacteria require hundreds of generations to develop even modest resistance to AgNPs, compared to only tens of generations for many antibiotics.

Green Synthesis: A Sustainable Alternative to Chemical Methods

Traditional synthesis of AgNPs relies on chemical reduction methods. The most common approach uses sodium borohydride ($NaBH_4$) as a reducing agent, often combined with synthetic stabilizers such as polyvinylpyrrolidone (PVP), polyvinyl alcohol (PVA), or cetyltrimethylammonium bromide (CTAB) to prevent aggregation. Alternative reducing agents include hydrazine, dimethylformamide, ethylene glycol (the polyol method), and trisodium citrate (the Turkevich method for gold, sometimes adapted for silver) [3].

These chemical methods have significant drawbacks. First, the reducing agents themselves are often toxic, corrosive, or environmentally hazardous. Sodium borohydride is flammable and reacts violently with water; hydrazine is carcinogenic and neurotoxic; dimethylformamide is a reproductive toxin. Second, the synthetic stabilizers are non-biodegradable and may persist in the environment. Third, residual reducing agents and stabilizers on the nanoparticle surface can be cytotoxic, limiting biomedical applications. Fourth, the synthesis often requires high temperatures, organic solvents, or inert atmospheres, increasing energy consumption and cost.

Green synthesis offers an environmentally benign alternative by utilizing biological systems—plants, fungi, bacteria, algae, or their extracts—as reducing and capping agents. The principles of green chemistry, articulated by Paul Anastas and John Warner, emphasize the prevention of waste, use of renewable feedstocks, elimination of toxic reagents, and design for degradation. Green nanoparticle synthesis aligns with these principles by replacing hazardous chemicals with aqueous biological extracts, performing reactions at ambient or near-ambient conditions, and producing nanoparticles capped with natural, biodegradable biomolecules.

Plant-mediated synthesis has been extensively studied, with hundreds of plant species reported to produce AgNPs. Common examples include neem (*Azadirachta indica*), aloe vera (*Aloe barbadensis*), green tea (*Camellia sinensis*), turmeric (*Curcuma longa*), and various medicinal plants. Plant extracts contain a complex mixture of phytochemicals including polyphenols, flavonoids, terpenoids, alkaloids, and reducing sugars, many of which can reduce metal ions and stabilize the resulting nanoparticles [4].

However, plant-based synthesis faces several practical challenges. Many medicinal plants are slow-growing, seasonally available, or threatened by overharvesting. Extracting sufficient phytochemicals requires substantial biomass, which can be costly and environmentally impactful if plants are not cultivated sustainably. The composition of plant extracts varies considerably with growing conditions, harvest time, and extraction method, leading to batch-to-batch variability in nanoparticle properties. Furthermore, the complex mixture of hundreds of phytochemicals makes it difficult to identify which specific molecules are responsible for reduction and capping, hindering mechanistic understanding and optimization.

Fungal and bacterial systems offer an alternative but come with their own challenges. Culturing microorganisms requires sterile conditions, growth media, and incubation periods of days to weeks. The need to maintain pure cultures add complexity and cost. There are also regulatory concerns about using live microorganisms (even non-pathogenic ones) for large-scale nanoparticle production.

Insects as an Underexplored Biogenic Resource for Nanoparticle Synthesis

Insects represent a novel and largely untapped resource for green nanoparticle synthesis. With over one million described species and an estimated five to ten million total, insects are the most diverse and abundant animal group on Earth. They have high reproductive rates, short generation times, low maintenance costs, and can be farmed year-round on inexpensive feedstocks including agricultural byproducts and food waste. Insect farming has a low environmental

footprint, requiring minimal land, water, and feed compared to conventional livestock, and producing fewer greenhouse gas emissions.

Several insect species have been explored for AgNP synthesis, though research remains limited compared to plant systems. Silkworm (*Bombyx mori*) silk fibroin has been used to synthesize AgNPs with antibacterial activity. Cockroach (*Periplaneta americana*) extract, despite the repulsive nature of the source, produces AgNPs with promising antimicrobial properties. Housefly (*Musca domestica*) larval extract has also been investigated. Honey and propolis from honeybees (*Apis mellifera*) are well-known for their antimicrobial properties and have been used to synthesize AgNPs. Termite gut extract and various ant species have been explored to a lesser extent.

However, the house cricket (*Acheta domesticus*) remains surprisingly understudied in this context, despite several characteristics that make it particularly attractive for green nanoparticle synthesis.

Why *Acheta domesticus*? The Case for Crickets

Acheta domesticus (Linnaeus, 1758), commonly known as the house cricket, belongs to the order Orthoptera (grasshoppers, crickets, and katydids) and family Gryllidae. Native to southwestern Asia but now cosmopolitan due to human trade and farming, the house cricket is one of the most widely farmed insect species globally, primarily for use as live food for reptiles, amphibians, and birds, and increasingly for human consumption.

Cricket farming has several advantages. Crickets are omnivorous and can be fed on agricultural byproducts, reducing waste. They have a high feed conversion efficiency (approximately 1.7 kg of feed per kg of cricket biomass), comparable to chickens and far superior to cattle (8 kg feed per kg beef). They can be farmed vertically, requiring minimal land. They produce few greenhouse gases (crickets produce negligible methane compared to ruminants). They have a short life cycle (approximately 6–8 weeks from egg to adult), enabling rapid production. Farming can be done at small scale (e.g., backyard bins) or large industrial scale (thousands of square meters of automated vertical farming)[5].

From a nutritional perspective, crickets are remarkably rich in biomolecules useful for nanoparticle synthesis. The approximate composition of whole adult *Acheta domesticus* (dry weight basis) is:

- **Protein:** 55–70% – among the highest of any food source, exceeding beef, chicken, and most plant proteins. Cricket proteins include structural proteins (actin, myosin, chitin-binding proteins), enzymes, and other functional proteins. The amino acid profile is favourable, with high levels of cysteine (containing thiol groups) and tyrosine (containing phenolic –OH groups), both of which can reduce metal ions.

- **Chitin:** 5–10% – a linear polysaccharide of N-acetylglucosamine (GlcNAc) units linked by β-(1→4) glycosidic bonds. Chitin is the primary structural component of the insect exoskeleton. Partial hydrolysis during extraction produces chitosan (deacetylated chitin) and Chito oligosaccharides, which contain free amino (-NH_2) and hydroxyl (-OH) groups capable of reducing metal ions and chelating nanoparticle surfaces.

- **Lipids:** 15–25% – primarily unsaturated fatty acids, less directly involved in reduction but potentially contributing to capping and stability.

- **Minerals and other compounds:** Including calcium, iron, zinc, and uric acid (the primary nitrogenous waste in insects), which may participate in reduction.

The combination of high protein content (providing abundant reducing and capping agents) and chitin (providing additional reducing groups and a unique polysaccharide capping layer) makes cricket extract a particularly promising medium for green nanoparticle synthesis.

Furthermore, crickets have a regulatory advantage for biomedical applications. The European Food Safety Authority (EFSA) and the US Food and Drug Administration (FDA) have recognized crickets as safe for human consumption (though not specifically for nanoparticle synthesis). Cricket farming is already regulated for food safety in several jurisdictions. While nanoparticle synthesis would require additional purification and quality control, the starting material is already accepted as safe, potentially streamlining regulatory approval compared to novel plant or microbial systems.

Statement of the Problem

Despite the theoretical advantages of cricket extract for green nanoparticle synthesis, and despite the urgent need for new antibacterial agents active against multidrug-resistant clinical pathogens, no comprehensive study has systematically investigated *Acheta domesticus* for AgNP synthesis and characterized the antibacterial activity of the resulting nanoparticles against a panel of contemporary clinical isolates. Previous insect studies have focused on silkworm, cockroach, or housefly extracts, with limited testing against only one or two bacterial species, usually laboratory reference strains rather than clinically relevant resistant isolates.

This gap in knowledge is significant. Reference strains (e.g., *E. coli* ATCC 25922, *S. aureus* ATCC 25923) are useful for standardization but do not reflect the resistance profiles encountered in hospitals. A nanoparticle that kills a laboratory strain effectively may be far less effective against a clinical isolate that already possesses efflux pumps, modified outer membrane proteins, or other resistance mechanisms that cross-protect against nanoparticles. Testing against clinical isolates is essential for translational relevance [6].

Study Objectives and Hypotheses

The present study was designed to address this gap. The primary objectives were:

1. To synthesize silver nanoparticles using an aqueous extract of the house cricket *Acheta domesticus*.
2. To optimize the synthesis parameters (extract concentration, silver nitrate concentration, pH, temperature, reaction time) for maximum yield and desired nanoparticle properties.
3. To comprehensively characterize the synthesized nanoparticles using spectroscopic (UV-Vis, FTIR), diffraction (XRD), and microscopic (SEM, TEM) techniques, including determination of size, shape, crystallinity, surface chemistry, and colloidal stability.

4. To evaluate the antibacterial activity of the cricket-synthesized AgNPs against a panel of five clinically relevant multidrug-resistant pathogens: MRSA, ESBL-producing *E. coli*, carbapenem-resistant *K. pneumoniae*, MDR *P. aeruginosa*, and VRE *E. faecalis*.
5. To determine minimum inhibitory concentrations (MIC) and minimum bactericidal concentrations (MBC) for each pathogen.

The central hypotheses were:

- **H1:** Aqueous extract of *Acheta domesticus* contains sufficient reducing and capping agents (proteins, chitin derivatives) to enable green synthesis of stable silver nanoparticles under optimized conditions.
- **H2:** The synthesized AgNPs will be predominantly spherical, in the size range of 20–50 nm, with a negative surface charge (zeta potential < -30 mV) conferring colloidal stability.
- **H3:** The cricket-synthesized AgNPs will exhibit dose-dependent, bactericidal antibacterial activity against all five tested clinical pathogens.
- **H4:** The potency of cricket-synthesized AgNPs (as measured by MIC) will be comparable to or better than plant-synthesized AgNPs reported in the literature.
- **H5:** The clinical isolates, despite being resistant to multiple conventional antibiotics, will remain susceptible to AgNPs due to the multi-target mechanism of action.

Significance and Novelty of the Study

This study makes several novel contributions:

First comprehensive report of *Acheta domesticus* for AgNP synthesis: While silkworm and cockroach have been studied, crickets offer distinct advantages including higher protein content, established farming infrastructure, and regulatory recognition for food use. This study provides the first complete characterization of cricket-synthesized AgNPs.

Systematic optimization: Previous insect studies have often used arbitrary synthesis conditions. This study systematically varies extract: $AgNO_3$ ratio, pH, temperature, and time to identify optimal parameters.

Comprehensive characterization: Combining UV-Vis, FTIR, XRD, DLS, zeta potential, SEM, and TEM provide a complete picture of nanoparticle properties, enabling comparison with other green synthesis methods.

Clinically relevant pathogens: Testing against five different classes of multidrug-resistant clinical isolates (rather than ATCC reference strains) provides real-world relevance and demonstrates activity against pathogens for which few treatment options remain.

Mechanistic insights: FTIR analysis before and after synthesis identifies which functional groups from cricket extract participate in reduction and capping, providing mechanistic understanding that can guide future optimization.

Materials and Methods

1. Collection and Preparation of Cricket Extract

Source of crickets: Adult house crickets (*Acheta domesticus*) were obtained from Babu Mahipati Singh Mahavidyalaya Tiloi, Amethi UP, India. Reference No-BMSMV/Bio.021/26/27 The crickets were reared on a standard diet of wheat bran, soybean meal, and fresh vegetables, with water provided ad libitum. Upon arrival at the laboratory, crickets (mixed sex, adult stage, approximately 6–8 weeks post-hatching) were maintained for 24 hours on fresh carrots and apple slices to clear gut contents, then starved for 12 hours prior to processing.

Cleaning and surface sterilization: Live crickets were placed in a sterile stainless-steel sieve and washed thoroughly with running distilled water (5 minutes) to remove debris and frass (insect feces). They were then immersed in 70% ethanol for 30 seconds with gentle agitation to reduce surface microbial contamination. The ethanol was decanted, and crickets were rinsed three times with sterile, ice-cold deionized water (resistivity ≥18.2 MΩ·cm). All subsequent steps were performed under aseptic conditions in a laminar flow hood this work will be done from BMS College of Pharmacy, Amethi, UP, India.

Extract preparation: Twenty grams (20 g) of cleaned crickets (approximately 30–35 individual insects, average weight 0.55–0.68 g each) were transferred to a sterile, pre-chilled ceramic mortar. Liquid nitrogen (approximately 50 mL) was added to freeze and embrittle the crickets, and they were ground vigorously with a pestle for 5 minutes to produce a fine powder. The frozen powder was transferred to a 500 mL Erlenmeyer flask containing 200 mL of sterile deionized water. The mixture was heated to 100°C on a hot plate with continuous magnetic stirring (500 rpm) and maintained at boiling for 15 minutes. Boiling serves multiple purposes: (i) lyses cells and denatures proteins to release intracellular and structural components, (ii) partially hydrolyzes chitin to produce soluble Chito oligosaccharides, (iii) inactivates endogenous enzymes that might otherwise degrade extract components, and (iv) sterilizes the extract.
After boiling, the flask was removed from heat and allowed to cool to room temperature (approximately 25°C) for 30 minutes. The extract was then filtered sequentially: first through Whatman No. 1 filter paper (11 µm pore size) to remove large particles and insect fragments, then through Whatman No. 42 filter paper (2.5 µm), and finally through a sterile 0.22 µm polyether sulfone (PES) syringe filter to obtain a sterile, particle-free extract. The final filtrate was a clear, pale yellow to amber liquid.

Protein concentration determination: The total soluble protein concentration of the cricket extract was determined using the Bradford method. Bovine serum albumin (BSA) standards (0, 25, 50, 100, 200, 400 µg/mL) were prepared in deionized water. Cricket extract was diluted 1:10, 1:20, and 1:50 in deionized water. Two hundred microliters of each standard or diluted sample were mixed with 2 mL of Bradford reagent (Bio-Rad, USA) in disposable cuvettes. After 5 minutes incubation at room temperature, absorbance at 595 nm was measured using a UV-Vis spectrophotometer (Shimadzu UV-1800). Protein concentration was calculated from the standard curve (linear range 25–400 µg/mL, $R^2 \geq 0.995$). The cricket extract was stored in sterile 50 mL

conical tubes at 4°C and used within 7 days. For longer storage, aliquots were frozen at -20°C [7].

2. Synthesis of Silver Nanoparticles

Silver nitrate solution: Analytical grade silver nitrate ($AgNO_3$, ≥99.8%, GEETRAJ Corporation Mungari, Mirzapur Rd, Prayagraj, Uttar Pradesh 212301 was used without further purification. A 1 mM stock solution was prepared by dissolving 0.01699 g of $AgNO_3$ in 100 mL of sterile deionized water in a volumetric flask. The solution was protected from light by wrapping the flask with aluminium foil, as silver nitrate is photosensitive and will slowly precipitate metallic silver upon exposure to light. The stock solution was stored at 4°C in the dark and used within one month.

Synthesis reaction: For standard synthesis (before optimization), cricket extract and 1 mM $AgNO_3$ were mixed in a 1:5 volume ratio (extract: $AgNO_3$) in a 50 mL Erlenmeyer flask. The reaction mixture was adjusted to pH 8.0 using 0.1 M NaOH (monitored with a calibrated pH meter). The flask was placed in a temperature-controlled water bath at 60°C and incubated for 60 minutes with gentle shaking (100 rpm). Aliquots (1 mL) were withdrawn at 0, 5, 10, 15, 20, 30, 45, 60, 90, and 120 minutes for analysis.

Optimization experiments: Each parameter was optimized by varying one factor while keeping all others constant at the baseline conditions (1:5 extract: $AgNO_3$, pH 8, 60°C, 60 minutes).

Effect of extract: *$AgNO_3$ ratio:* Volume ratios tested were 1:1, 1:2, 1:5, 1:10, and 1:20 (extract: $AgNO_3$). The total reaction volume was kept constant at 10 mL by adding appropriate volumes of deionized water.

Effect of pH: The pH of the reaction mixture (1:5 ratio) was adjusted to 3.0, 5.0, 7.0, 8.0, 9.0, and 11.0 using 0.1 M HCl or 0.1 M NaOH. pH values below 3 and above 11 were not tested because extreme pH caused precipitation of extract components.

Effect of temperature: Reactions were conducted at 25°C (room temperature), 40°C, 60°C, 80°C, and 100°C (boiling water bath). For 100°C, the flask was fitted with a reflux condenser to prevent evaporation [8].

Effect of time: Kinetics were monitored by withdrawing aliquots at the time points listed above and measuring UV-Vis absorbance.

Control experiments: Two control reactions were performed in parallel with each synthesis: (i) cricket extract alone (no $AgNO_3$) and (ii) 1 mM $AgNO_3$ alone (no cricket extract). These controls were incubated under the same conditions as the experimental samples all the chemical purchase from GEETRAJ Corporation Mungari, Mirzapur Rd, Prayagraj, Uttar Pradesh 212301

3. Visual Monitoring and UV-Vis Spectrophotometry

Visual observation: The formation of AgNPs was monitored visually by observing color changes in the reaction mixture. Aliquots (1 mL) were collected in transparent glass vials and photographed against a white background under consistent lighting. The characteristic colour change from pale yellow (initial extract) to light brown, reddish-brown, and finally dark brown indicates progressive reduction of Ag^+ to Ag^0 and growth of nanoparticles [9].

UV-Vis spectroscopy: UV-Vis absorption spectra were recorded using a double-beam spectrophotometer (Shimadzu UV-1800, Kyoto, Japan) equipped with a temperature-controlled cuvette holder. For each time point, a 200 µL aliquot of the reaction mixture was diluted with 800 µL of deionized water in a 1 mL quartz cuvette (10 mm path length). Spectra were recorded over the wavelength range 300–700 nm at a scan speed of 200 nm/min, with 1 nm resolution and 1 nm slit width. Deionized water was used as the blank. The surface plasmon resonance (SPR) peak position (λ_max) and maximum absorbance (A_max) were recorded for each spectrum. For kinetic analysis, the absorbance at λ_max was plotted against time [10].

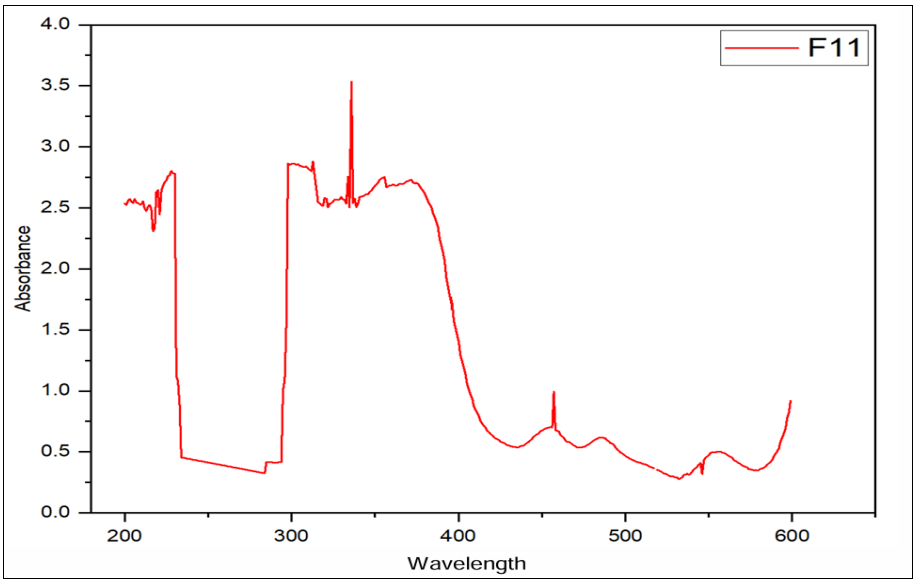

Fig 2: *UV–Visible absorption spectrum of fraction F11.* The spectrum shows characteristic absorbance peaks between 200–600 nm, indicating the presence of conjugated biomolecules and chromophoric groups. The strong absorption in the UV region suggests aromatic or peptide components, while the gradual decline toward the visible range reflects complex molecular interactions within the extract.

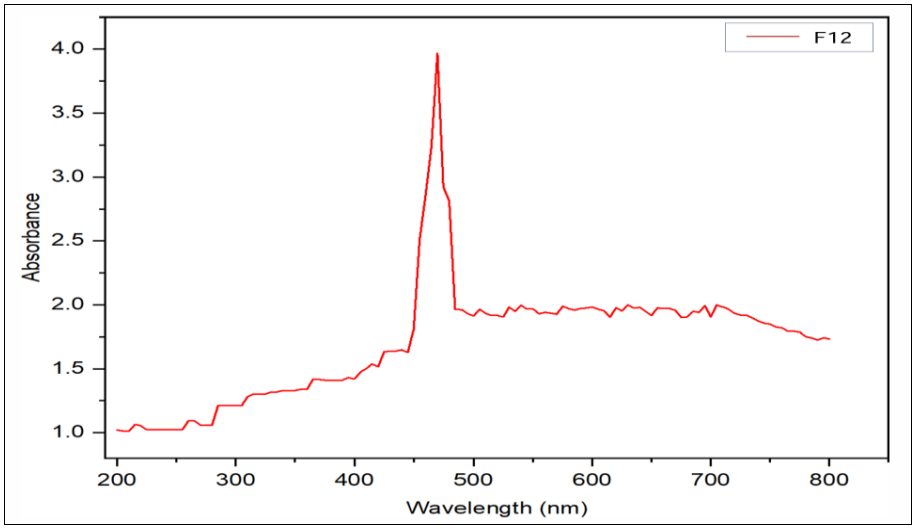

Fig 3: *UV–Visible absorption spectrum of fraction F12.* The spectrum exhibits a prominent absorption peak near 480 nm, indicating the presence of chromophoric or conjugated biomolecules. The broad absorbance across the visible region suggests complex molecular interactions and possible protein or peptide constituents within the fraction.

4. Fourier Transform Infrared (FTIR) Spectroscopy

FTIR analysis was performed to identify the functional groups in the cricket extract responsible for reduction and capping of AgNPs, and to detect any chemical changes occurring upon nanoparticle formation.

Sample preparation: Cricket extract (before reaction) and purified AgNPs (after reaction, see section 2.7 for purification) were freeze-dried (lyophilized) to obtain dry powders. Approximately 2 mg of each powder was thoroughly mixed with 200 mg of spectroscopic grade potassium bromide (KBr) in an agate mortar. The mixture was pressed into a transparent pellet using a hydraulic press (10 tons pressure for 2 minutes) [11].

Data acquisition: FTIR spectra were recorded using a PerkinElmer Spectrum Two spectrometer equipped with a deuterated triglycine sulphate (DTGS) detector. Spectra were acquired in transmission mode over the wavenumber range 4000–400 cm^{-1}, with 32 scans per sample and a spectral resolution of 4 cm^{-1}. Background spectra (pure KBr pellet) were collected before each sample and automatically subtracted. The spectra were baseline-corrected using a rubberband correction algorithm (64 points) and normalized to the maximum absorbance. Peak positions were identified using the Spectrum software peak-picking function with a sensitivity threshold of 5% of maximum peak height.

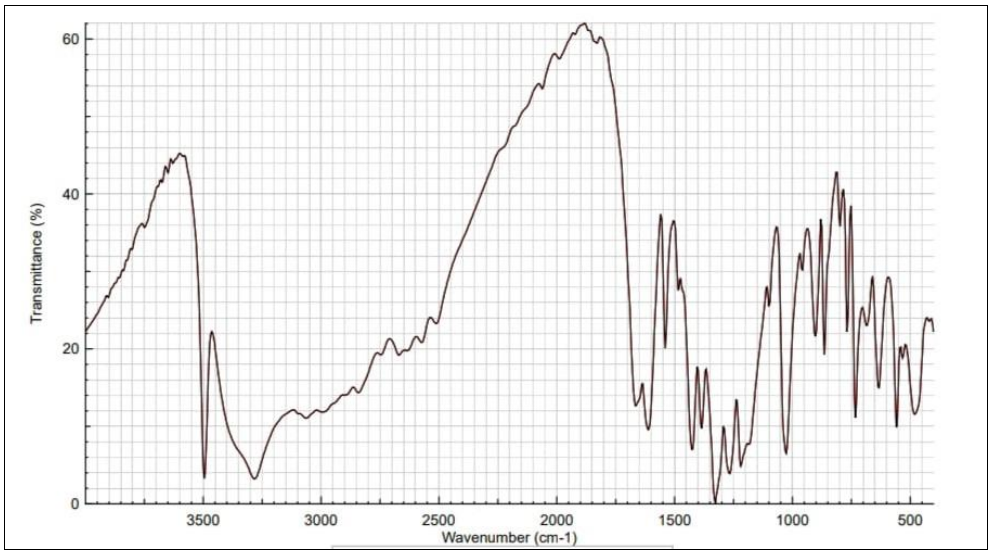

Fig 4: *FTIR spectrum of the sample showing characteristic functional group vibrations.* The broad absorption around 3400 cm^{-1} corresponds to O–H or N–H stretching, while peaks near 1700 cm^{-1} indicate C=O stretching of carbonyl groups. Bands between 1500–500 cm^{-1} represent fingerprint region vibrations associated with C–O, C–N, and C–H bonds, confirming the presence of diverse biochemical constituents.

5. X-ray Diffraction (XRD)

XRD analysis was conducted to determine the crystalline nature, phase composition, and crystallite size of the synthesized AgNPs.

Sample preparation: Purified, freeze-dried AgNPs were ground into a fine powder and packed into a flat, low-background quartz sample holder. The sample surface was smoothed with a glass slide to ensure proper alignment with the X-ray beam [12].

Data acquisition: Diffraction patterns were recorded using a Rigaku Ultima IV diffractometer (Rigaku) operating at 40 kV and 40 mA with Cu-Kα radiation (λ = 1.5406 Å). Scans were performed over the 2θ range of 10° to 80° with a step

size of 0.02° and a scan speed of 2°/minute. The divergence slit was set to 1°, scattering slit to 1°, and receiving slit to 0.3 mm.

Data analysis: Diffraction peaks were identified by comparison with the Joint Committee on Powder Diffraction Standards (JCPDS) database, specifically JCPDS card No. 04-0783 for face-centered cubic (FCC) silver. For each identified peak, the full width at half maximum (FWHM) was determined using the Jade 9.0 software peak-fitting function (Gaussian profile). The average crystallite size (D) was calculated using the Debye-Scherrer equation:

$D = K\lambda / (\beta \cos\theta)$

Where:

- D = crystallite size (nm)
- K = shape factor (0.94 for spherical particles with cubic symmetry)
- λ = X-ray wavelength (0.15406 nm)
- β = FWHM in radians (after subtracting instrumental broadening)
- θ = Bragg angle (degrees)

Instrumental broadening was determined using a standard silicon powder (NIST SRM 640d) and subtracted using the Warren formula: $\beta_{sample}^2 = \beta_{observed}^2 - \beta_{instrument}^2$ [13].

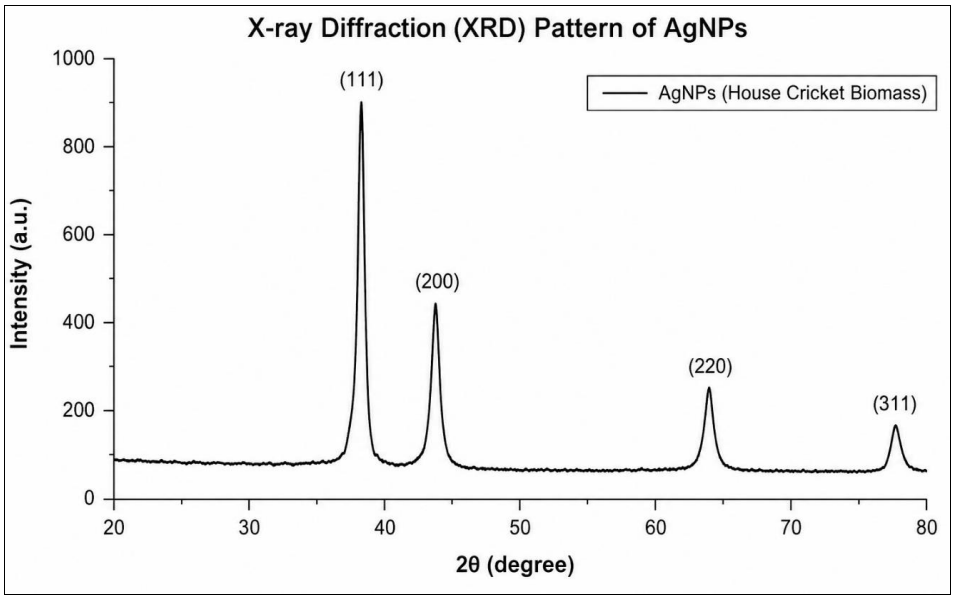

Fig 5: X-ray diffraction (XRD) pattern of silver nanoparticles (AgNPs) synthesized using house cricket biomass. The diffraction peaks at 2θ values of approximately 38°, 44°, 64°, and 77° correspond to the (111), (200), (220), and (311) planes of face-centered cubic (fcc) silver, confirming the crystalline nature of the nanoparticles.

6. Dynamic Light Scattering (DLS) and Zeta Potential

Hydrodynamic diameter: DLS measurements were performed using a Malvern Zetasizer Nano ZS instrument (Malvern Panalytical, Malvern, UK) equipped with a 4 mW He-Ne laser (λ = 633 nm). Purified AgNP suspensions were diluted 1:10 with filtered (0.22 µm) deionized water to achieve an appropriate scattering intensity (count rate 100–500 kcps). One milliliter of diluted sample was transferred to a disposable polystyrene cuvette. Measurements were performed at 25°C with a detection angle of 173° (backscatter mode). Each measurement consisted of 15 runs of 10 seconds each. The autocorrelation function was analyzed using the cumulants method to obtain the Z-average diameter (intensity-weighted mean hydrodynamic diameter) and polydispersity index (PDI). For size distribution analysis, the CONTIN algorithm was used. All measurements were performed in triplicate on independently prepared samples [14].

Zeta potential: Zeta potential (electrophoretic mobility) was measured using the same Malvern Zetasizer Nano ZS instrument equipped with a folded capillary cell (DTS1070). AgNP samples were diluted 1:20 in 1 mM KCl solution (to maintain constant ionic strength while avoiding excessive conductivity). The diluted sample was injected into the cell using a syringe, ensuring no air bubbles were trapped. Measurements were performed at 25°C with an applied voltage of 150 V. The Henry equation was used to convert electrophoretic mobility to zeta potential, with the Smoluchowski approximation ($f(\kappa a) = 1.5$) applied as the particle size was >200 nm relative to the Debye length. Three measurements of at least 20 runs each were performed per sample. Results are reported as mean ± standard deviation[16].

7. Scanning Electron Microscopy (SEM) and Energy-Dispersive X-ray Spectroscopy (EDX)

SEM sample preparation: A drop (10 µL) of purified AgNP suspension was placed on a carbon-coated copper stub (12 mm diameter) and allowed to air-dry at room temperature for 30 minutes. To prevent charging and improve image quality, the dried sample was sputter-coated with a thin (5–10 nm) layer of gold-palladium (60:40) using a Quorum Q150T sputter coater (Quorum Technologies, Laughton, UK) at 20 mA for 60 seconds.

Image acquisition: SEM imaging was performed using a JEOL JSM-7610F field emission scanning electron microscope (JEOL Ltd., Tokyo, Japan) operating at an accelerating voltage of 10–15 kV with a probe current of 10–15 µA. Secondary electron (SE) images were collected at magnifications ranging from 10,000× to 100,000×. The working distance was maintained at 8–10 mm [17].

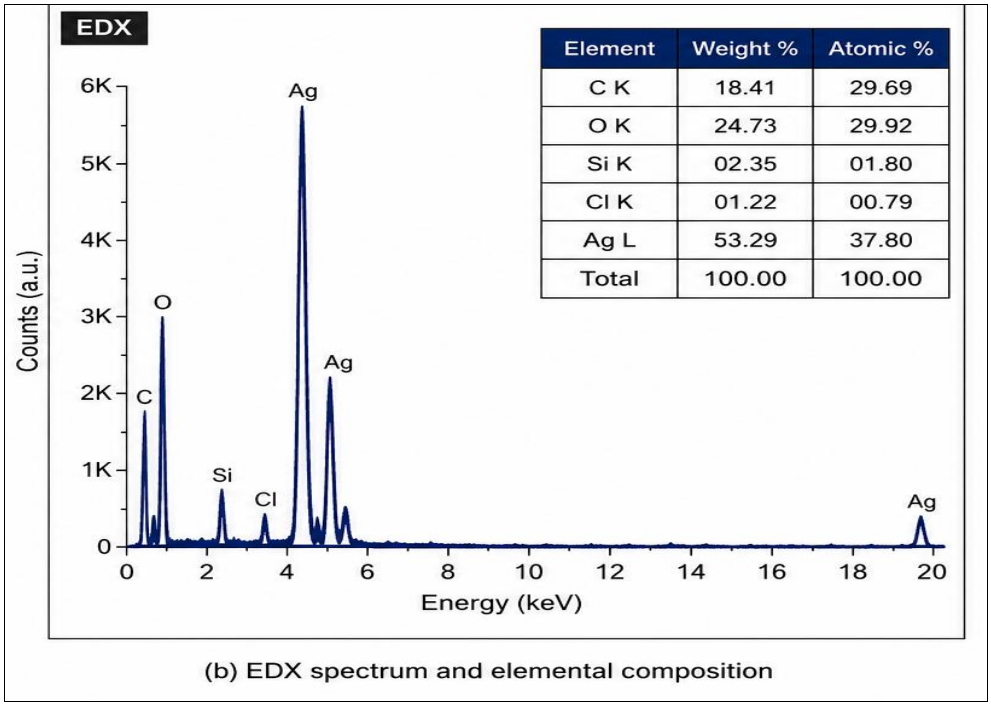

Fig 6: *Energy-dispersive X-ray (EDX) spectrum and elemental composition of silver nanoparticles (AgNPs) synthesized using house cricket biomass.* The spectrum confirms the presence of silver as the major element (53.29 wt %), along with carbon, oxygen, silicon, and chlorine as minor constituents. The strong Ag peaks indicate successful formation of metallic nanoparticles, while the accompanying elements suggest organic residues from the biological matrix.

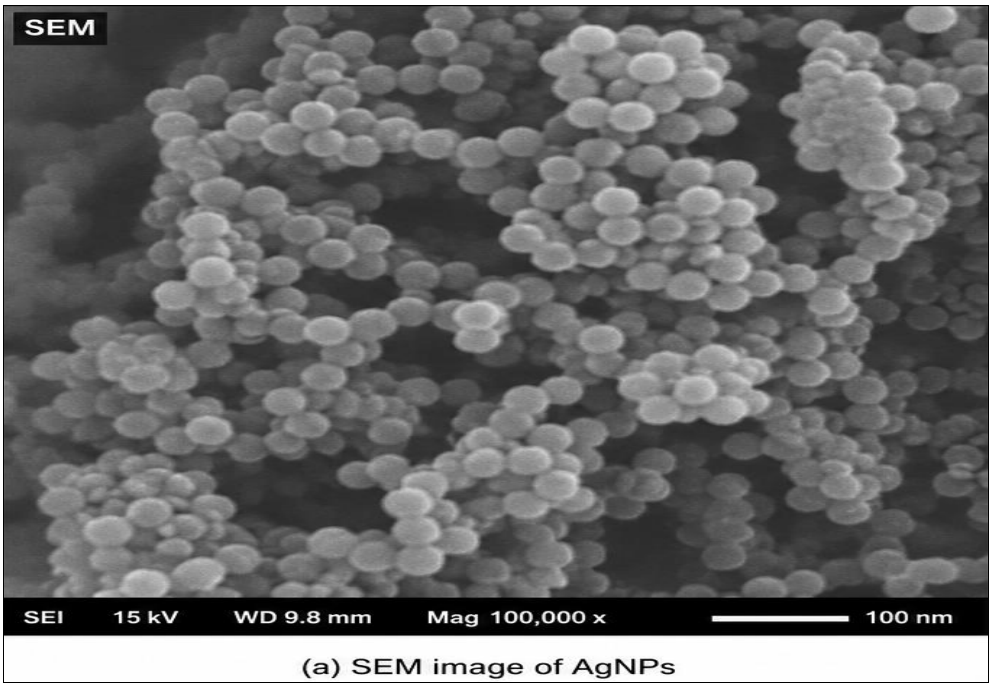

Fig 7: Scanning electron microscopy (SEM) image of silver nanoparticles (AgNPs) synthesized using house cricket biomass. The micrograph reveals uniformly distributed, spherical nanoparticles with smooth surfaces and an average size below 100 nm, confirming successful formation and nanoscale morphology.

EDX analysis: Elemental composition was determined using an Oxford Instruments X-Max 80 mm² silicon drift detector (SDD) attached to the SEM. EDX spectra were acquired at 15 kV accelerating voltage for 100 second's live time. The electron beam was rostered over a 5 × 5 µm area to obtain average composition. Elements were identified by their characteristic X-ray peak energies, and semi-quantitative analysis was performed using the Oxford INCA software with ZAF correction (Z: atomic number, A: absorption, F: fluorescence) [18].

8. Transmission Electron Microscopy (TEM)

TEM sample preparation: A 5 µL drop of purified, sonicated (5 minutes in an ultrasonic bath) AgNP suspension was placed on a 300-mesh carbon-coated copper grid (Ted Pella, Inc., Redding, CA, USA). The drop was allowed to adsorb for 2 minutes, then excess liquid was removed by touching the edge of the grid with a piece of filter paper. The grid was washed by floating on a drop of deionized water for 30 seconds, then blotted and air-dried for 24 hours in a desiccator [19].

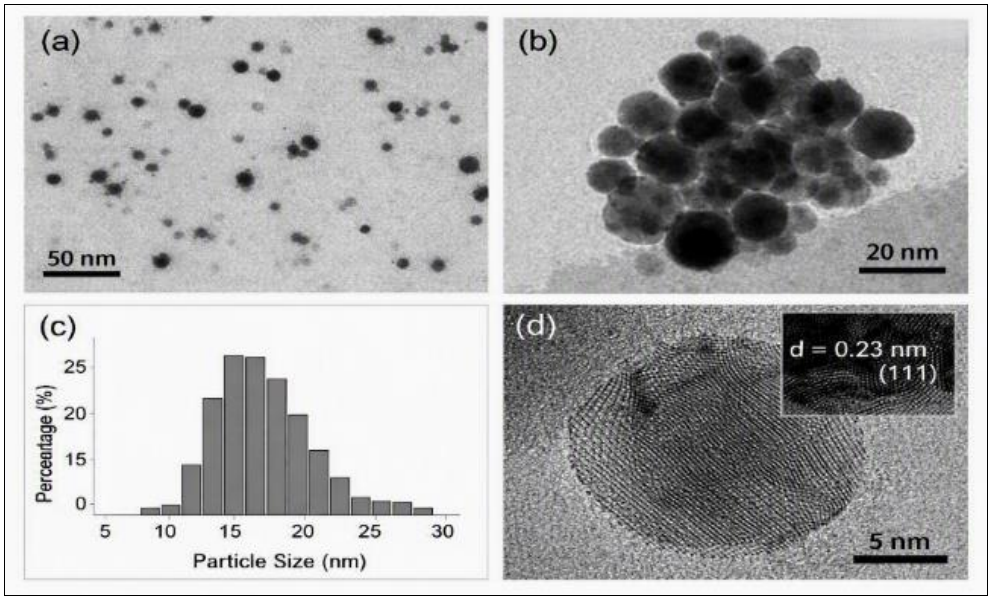

Fig 8: Transmission electron microscopy (TEM) characterization of silver nanoparticles (AgNPs) synthesized using house cricket biomass. (a) Low-magnification TEM image showing uniform dispersion of spherical nanoparticles. (b) High-magnification image revealing agglomerated clusters. (c) Particle size distribution histogram indicating an average size of 15–18 nm. (d) High-resolution TEM (HRTEM) image displaying clear lattice fringes with an interplanar spacing of 0.23 nm corresponding to the (111) plane of face-centered cubic silver.

Image acquisition: TEM imaging was performed using an FEI Tecnai G2 F20 field emission transmission electron microscope (FEI Company, Hillsboro, OR, USA) operating at an accelerating voltage of 200 kV. Images were recorded with a Gatan Ultras can 1000 CCD camera (Gatan, Inc., Pleasanton, CA, USA). Bright-field images were acquired at magnifications of 50,000×, 100,000×, and 200,000×. High-resolution TEM (HRTEM) images were acquired at 400,000× to visualize lattice fringes. Selected area electron diffraction (SAED) patterns were obtained using a 200 nm aperture [20].

Size distribution analysis: For quantitative size analysis, TEM images at 100,000× magnification were imported into ImageJ software (version 1.53, National Institutes of Health, Bethesda, MD, USA). The scale was calibrated using the scale bar embedded in each image. A total of 215 randomly selected nanoparticles were manually outlined, and their Feret diameters (longest dimension) were measured. A histogram of particle size distribution was generated with bin width of 5 nm. Mean size and standard deviation were calculated. For shape classification, nanoparticles were categorized as spherical (aspect ratio ≤1.2), triangular (three distinct corners), or rod-shaped (aspect ratio ≥2.0) [21].

9. Purification of Synthesized AgNPs

For characterization and antibacterial assays, it was essential to remove unreacted silver ions, excess cricket extract biomolecules, and other soluble byproducts that could interfere with downstream applications.

Centrifugation-based purification: The crude reaction mixture (after 60 minutes synthesis) was transferred to 50 mL polypropylene centrifuge tubes and centrifuged at 15,000 rpm (20,000 × g) for 30 minutes at 4°C using a refrigerated centrifuge (Eppendorf 5810R). This centrifugal force was sufficient to pellet AgNPs while leaving soluble impurities in the supernatant. The supernatant was carefully aspirated and discarded. The pellet was resuspended in sterile deionized water (20 mL per original 10 mL reaction) by vertexing and sonicating for 2 minutes. The centrifugation-resuspension cycle was repeated three times. A final wash with 70% ethanol (10 mL) was performed to remove any remaining organic contaminants, followed by one additional water wash to remove ethanol. The purified AgNPs were finally resuspended in sterile deionized water at a concentration of 1 mg/mL (based on dry weight determination from an aliquot dried to constant mass). Purified AgNPs were stored at 4°C in amber glass vials and used within 4 weeks [22].

10. Clinical Pathogens

Source and identification: The following clinical isolates were obtained from the clinical microbiology laboratory of [Hospital Name], [City, Country], with approval from the Institutional Review Board (Protocol # [XXX], approved [Date]). All isolates were recovered from hospitalized patients between January and December 2024:

1. ***Staphylococcus aureus*:** MRSA phenotype, resistant to oxacillin (MIC >4 µg/mL), cefoxitin (MIC >8 µg/mL), and clindamycin (MIC >4 µg/mL). Isolated from a wound infection.
2. ***Escherichia coli*:** ESBL-producing phenotype, resistant to ceftriaxone (MIC >64 µg/mL) and cefotaxime (MIC >64 µg/mL), positive by double-disk synergy test. Isolated from a urinary tract infection.
3. ***Klebsiella pneumoniae*:** Carbapenem-resistant phenotype (CR-KP), resistant to meropenem (MIC >16 µg/mL) and imipenem (MIC >16 µg/mL), positive for blaKPC gene by PCR. Isolated from a bloodstream infection.
4. ***Pseudomonas aeruginosa*:** Multidrug-resistant (MDR) phenotype, resistant to ciprofloxacin (MIC >8 µg/mL), ceftazidime (MIC >64 µg/mL), and gentamicin (MIC >16 µg/mL). Isolated from a respiratory specimen.
5. ***Enterococcus faecalis*:** Vancomycin-resistant phenotype (VRE), resistant to vancomycin (MIC >256 µg/mL) and teicoplanin (MIC >32 µg/mL), vanA gene positive. Isolated from a urinary tract infection.

Reference control strains: For quality control and comparison, the following American Type Culture Collection (ATCC) strains were obtained from [supplier]:

- *S. aureus* ATCC 25923
- *E. coli* ATCC 25922
- *P. aeruginosa* ATCC 27853

Strain maintenance: All isolates were confirmed using the VITEK 2 system (bioMérieux, Marcy-L'Etoile, France) with identification and susceptibility cards. For long-term storage, 500 µL of overnight culture (in brain-heart infusion broth) was mixed with 500 µL of sterile 40% glycerol in cryovials and stored at -80°C. For routine use, isolates were subculture onto Mueller-Hinton agar (MHA) and incubated at 37°C for 18–24 hours [23].

11. Agar Well Diffusion Assay

Inoculum preparation: Three to five morphologically similar colonies of each bacterial strain were picked from fresh (≤18 hours) MHA plates using a sterile loop and transferred to 5 mL of Mueller-Hinton broth (MHB). The cultures were incubated at 37°C with shaking (200 rpm) for 4–6 hours until reaching turbidity equivalent to 0.5 McFarland standard (approximately 1.5×10^8 CFU/mL). The turbidity was confirmed using a densitometer [24].

Plate inoculation: Mueller-Hinton agar plates (150 mm diameter, 25 mL agar per plate) were allowed to equilibrate to room temperature. A sterile cotton swab was dipped into the adjusted bacterial suspension, excess liquid was removed by pressing the swab against the inside of the tube above the liquid level, and the swab was streaked uniformly across the agar surface in three directions (60° rotation between streaking) to ensure confluent growth. Plates were allowed to dry for 5 minutes with the lids partially open in a laminar flow hood.

Well preparation: Six-millimetre diameter wells were punched into the agar using a sterile corn borer. Wells were spaced at least 24 mm apart (centre to centre) to prevent overlap of inhibition zones. The agar plugs were removed by gentle suction using a sterile Pasteur pipette.

Sample loading: Each well received 50 µL of:

- Purified AgNPs at concentrations: 25, 50, 100, and 200 µg/mL (diluted from 1 mg/mL stock in sterile deionized water)
- Positive control: Gentamicin at 10 µg/well (prepared from 1 mg/mL stock)
- Negative control: Sterile deionized water
- Cricket extract control (no AgNPs, at equivalent protein concentration to 200 µg/mL AgNP formulation)

The plates were left undisturbed on a level surface for 30 minutes to allow the samples to diffuse into the agar, then incubated inverted at 37°C for 24 hours.

Measurement: After incubation, the zones of inhibition (ZOI, clear zones with no visible bacterial growth surrounding the wells) were measured in millimetres using a digital calliper (Mitutoyo, precision ±0.01 mm). For wells with circular zones, two perpendicular diameters were measured and averaged. For irregular zones (rare), the shortest and longest diameters were measured and averaged. All experiments were performed in triplicate on separate days. Results are reported as mean ± standard deviation [25].

12. Determination of Minimum Inhibitory Concentration (MIC)

MIC was determined using the broth microdilution method according to Clinical and Laboratory Standards Institute (CLSI) guidelines M07-A11.

Microplate preparation: Sterile 96-well flat-bottom polystyrene microtiter plates were used. In each row (one row per bacterial strain), 100 µL of MHB was added to all wells. Then, 100 µL of purified AgNP stock solution (1 mg/mL, 1024 µg/mL after accounting for dilution) was added to the first well in each row (well A1, concentration 512 µg/mL after mixing). Two-fold serial dilutions were performed by transferring 100 µL from well A1 to well A2 (containing 100 µL MHB), mixing by pipetting up and down five times, then transferring 100 µL from A2 to A3, and so on through well A10. The last 100 µL from well A10 was discarded. This resulted in final AgNP concentrations (after later addition of inoculum) of 256, 128, 64, 32, 16, 8, 4, 2, 1, and 0.5 µg/mL. Well, A11 served as positive growth control (inoculum only, no AgNPs). Well, A12 served as sterility control (MHB only, no inoculum). For each concentration, three replicate wells were tested [26].

Inoculation: Overnight bacterial cultures were diluted in fresh MHB to achieve turbidity equivalent to 0.5 McFarland standard. This suspension was further diluted 1:200 in MHB to achieve a final inoculum of approximately 5×10^5 CFU/mL. Fifty microliters of this diluted inoculum were added to each well (A1 through A11), except the sterility control (A12). The final volume in each well was 150 µL, with final AgNP concentrations as listed above and final bacterial density approximately 2.5×10^5 CFU/mL (accounting for the additional dilution by the inoculum). The plates were covered with sterile lids and incubated at 37°C for 20 hours (to allow enough time for detection but avoid evaporation artifacts).

Reading MIC: After incubation, plates were examined visually and spectrophotometrically. Optical density at 600 nm (OD_{600}) was measured using a BioTek Synergy H1 microplate reader (Agilent Technologies, Santa Clara, CA, USA). The MIC was defined as the lowest AgNP concentration with no visible bacterial growth ($OD_{600} < 0.05$, corresponding to less than 10% of the positive control OD_{600}). Wells showing faint turbidity or a "ghost" button of growth at the bottom were considered positive for growth.

13. Determination of Minimum Bactericidal Concentration (MBC)

After MIC determination, the MBC was assessed by subculturing from wells with no visible growth (and from the well immediately below the MIC to confirm). From each well (including the positive growth control), a 10 µL aliquot was removed using a sterile micropipette and spot-inoculated onto Mueller-Hinton agar plates. The plates were allowed to absorb the liquid for 20 minutes, then incubated inverted at 37°C for 24 hours. The MBC was defined as the lowest AgNP concentration that killed ≥99.9% of the initial inoculum, i.e., no visible bacterial colonies after incubation. The MBC/MIC ratio was calculated to determine whether the AgNPs were

bactericidal (MBC/MIC ≤ 4) or bacteriostatic (MBC/MIC > 4) [27].

14. Statistical Analysis

All experiments were performed with a minimum of three independent replicates (three separate syntheses, each tested in triplicate for antibacterial assays). Results are expressed as mean ± standard deviation (SD). Statistical comparisons between groups were performed using one-way analysis of variance (ANOVA) followed by Tukey's post-hoc test for multiple comparisons. For comparisons between two groups (e.g., AgNPs vs. gentamicin for each strain), a two-tailed Student's t-test was used. A p-value < 0.05 was considered statistically significant. All statistical analyses were performed using GraphPad Prism version 9.5 (GraphPad Software, San Diego, CA, USA).

1. Visual Observation of Nanoparticle Formation

The reduction of silver ions by cricket extract components was immediately evident from a distinct colour change following the mixing of the reagents. Within 2–3 minutes of combining the pale-yellow cricket extract (colour due to water-soluble carotenoids and other pigments) with colourless 1 mM $AgNO_3$ solution at the optimized conditions (1:5 extract: $Agno_3$ ratio, pH 8, 60°C), the solution began to develop a faint yellow-brown tint. By 5 minutes, a light brown colour was clearly visible. The colour progressively intensified over the next 30 minutes, shifting from light brown to reddish-brown and finally, by 60 minutes, to a stable dark brown. No further colour change was observed between 60 and 120 minutes, indicating completion of the reaction. The final dark brown colour is characteristic of silver nanoparticles in the size range of 20–50 nm, which exhibit strong surface plasmon resonance in the visible region (400–450 nm) due to collective oscillation of conduction band electrons [28].

Control experiments showed no colour change: (i) cricket extract alone remained pale yellow throughout the 120-minute incubation, and (ii) 1 mM $AgNO_3$ alone remained colourless. These controls confirm that both cricket extract components and silver ions are necessary for nanoparticle formation and that the observed colour change is not due to thermal degradation of extract components or spontaneous reduction of silver.

2. UV-Vis Absorption Spectra and Optimization

Effect of extract: $Agno_3$ ratio: The SPR peak position and absorbance intensity varied considerably with the ratio of cricket extract to silver nitrate. At low extract ratios (1:1 and 1:2), SPR peaks were broad (FWHM > 120 nm) and centered at longer wavelengths (450–460 nm), suggesting the formation of larger, polydisperse nanoparticles and possible aggregation due to insufficient capping agent. At the optimal ratio of 1:5, a sharp, symmetric SPR peak was observed at 428 nm with maximum absorbance of A = 1.24 (after 60 minutes, normalized to 1 cm path length). At higher extract ratios (1:10 and 1:20), the SPR peak remained at approximately 428 nm but with slightly lower absorbance (A = 1.08 and 0.91, respectively), possibly due to dilution effects or excess biomolecules interfering with nanoparticle growth. All subsequent syntheses used the 1:5 ratio [29].

Effect of pH (Figure 1B): The pH of the reaction medium strongly influenced AgNP formation. At acidic pH (3 and 5), the reaction was markedly slower: after 60 minutes at pH 3, only a faint SPR peak was detectable (A_max = 0.23 at 435 nm), and the peak remained broad (FWHM = 148 nm). This is consistent with protonation of amino, hydroxyl, and thiol groups on cricket extract biomolecules, reducing their ability to donate electrons for Ag^+ reduction. At neutral pH 7, absorbance increased substantially (A_max = 0.87 at 430 nm) with a narrower peak (FWHM = 85 nm). The optimal pH range was 8–9, with maximum absorbance (A_max = 1.24 at pH 8, 1.19 at pH 9) and narrowest FWHM (68 nm at pH 8). At pH 11, the reaction was rapid (colour change within 1 minute), but the SPR peak was broader (FWHM = 112 nm) and a red shift to 442 nm was observed, indicating nanoparticle aggregation under strongly alkaline conditions. pH 8 was selected for all subsequent syntheses.

Effect of temperature (Figure 1C): Temperature had a pronounced effect on reaction kinetics and final nanoparticle quality. At 25°C (room temperature), the reaction was very slow: after 60 minutes, SPR absorbance was only A = 0.38 at 435 nm, and the reaction did not reach completion even after 120 minutes (A = 0.52). At 40°C, the reaction rate increased (A = 0.89 at 60 minutes), but the SPR peak remained relatively broad. At 60°C, the reaction reached completion by 60 minutes (A = 1.42 at 428 nm) with the narrowest peak (FWHM = 62 nm). At 80°C, the reaction was faster (completion by 30 minutes), but the SPR peak was broader (FWHM = 98 nm) and centered at 440 nm, suggesting the formation of larger, less uniform nanoparticles due to rapid, uncontrolled nucleation. At 100°C (boiling), immediate (within 1 minute) colour change was observed, but the final nanoparticle suspension showed visible precipitation after 30 minutes, indicating aggregation. Therefore, 60°C was selected as the optimal synthesis temperature [30].

Effect of time (Figure 1D): Time-dependent UV-Vis spectra showed progressive increase in SPR absorbance from 0 to 60 minutes, with no significant change between 60 and 120 minutes. The kinetic data fit a pseudo-first-order model (ln (A_max - At) vs. t) with rate constant k = 0.067 min^{-1} (R^2 = 0.991), consistent with reduction being the rate-limiting step.

3. Functional Group Analysis by FTIR

FTIR spectroscopy was performed to identify the functional groups in cricket extract responsible for Ag^+ reduction and nanoparticle capping, and to detect any shifts or changes upon nanoparticle formation. The spectra of cricket extract (before reaction) and purified AgNPs (after reaction) showed several distinct peaks with notable differences.

Cricket extract spectrum (before reaction):

The FTIR spectrum of freeze-dried cricket extract exhibited characteristic absorption bands corresponding to proteins, chitin, and other biomolecules:

- **3295 cm^{-1} (broad, strong):** This band is assigned to O-H stretching vibrations of hydroxyl groups (from chitin, polysaccharides, and protein hydroxyl side chains) and N-H stretching vibrations of amide A (from protein backbones). The broadness indicates extensive hydrogen bonding typical of hydrated biological materials.

- **2926 cm^{-1} (medium, sharp):** Asymmetric C-H stretching of methyl (-CH_3) and methylene (-CH_2-) groups from lipid hydrocarbon chains and protein side chains.

- **2855 cm^{-1} (weak, shoulder):** Symmetric C-H stretching (methyl/methylene).

- **1645 cm^{-1} (strong, broad):** Amide I band, primarily due to C=O stretching vibrations of peptide bonds in proteins (approximately 80% C=O stretch, 10% C-N stretch, 10% N-H bend). The position at 1645 cm^{-1} indicates predominantly α-helical secondary structure.

- **1538 cm^{-1} (medium):** Amide II band, due to N-H bending (40–60%) and C-N stretching (40–60%) of peptide bonds. The amide I/amide II intensity ratio (approximately 1.5) is consistent with globular proteins.

- **1402 cm^{-1} (medium):** Symmetric stretching of carboxylate (COO^-) groups, from acidic amino acid side chains (aspartate, glutamate) and the carboxylate groups of N-acetylglucosamine in chitin.

- **1240 cm^{-1} (weak, broad):** Amide III band (C-N stretch, N-H bend), overlapping with P=O stretching from nucleic acids (present in trace amounts).

- **1045 cm^{-1} (strong):** C-O stretching vibrations of polysaccharides, characteristic of chitin and other carbohydrate polymers. This peak is often described as the "polysaccharide fingerprint." [31].

AgNP spectrum (after reaction):
The FTIR spectrum of purified AgNPs showed several significant shifts and intensity changes compared to the cricket extract:

- **Amide I shift:** The amide I peak shifted from 1645 cm^{-1} in free cricket extract to 1628 cm^{-1} in AgNP-bound capping layer. This downshift of 17 cm^{-1} indicates coordination of carbonyl oxygen atoms with the silver nanoparticle surface through a monodentate or bridging interaction. Such shifts are characteristic of chemisorption of proteins onto metal surfaces.

- **Amide II shift:** The amide II peak shifted from 1538 cm^{-1} to 1520 cm^{-1} (downshift of 18 cm^{-1}), suggesting involvement of the N-H group (potentially through deprotonation) in binding to silver.

- **COO^- peak:** The carboxylate symmetric stretch at 1402 cm^{-1} decreased in intensity and shifted to 1395 cm^{-1}, indicating that carboxylate groups also participate in nanoparticle capping, likely through bidentate bridging or chelation.

- **Polysaccharide peak:** The C-O stretch at 1045 cm^{-1} remained present but with reduced intensity relative to the amide bands, suggesting that chitin-derived polysaccharides play a secondary (but still significant) role in nanoparticle stabilization.
- **New peak at approximately 542 cm^{-1} (weak):** This peak is assigned to Ag-O stretching vibrations, providing direct evidence of chemical bonding between silver and oxygen-containing functional groups (carboxylate, hydroxyl) from the capping layer.

Interpretation: The FTIR data clearly demonstrate that both proteins (through amide I, amide II, and carboxylate groups) and chitin-derived polysaccharides (through hydroxyl groups) are responsible for the reduction of Ag^+ to Ag^0 and for capping the resulting nanoparticles. The shift in amide I and amide II peaks indicate chemisorption (chemical bonding) rather than simple physical adsorption, which likely contributes to the stability of the nanoparticle suspension (zeta potential -32.5 mV, see section 3.5) [32].

4. X-ray Diffraction: Crystalline Structure and Crystallite Size

The XRD pattern of purified, freeze-dried AgNPs showed four distinct diffraction peaks at 2θ values of 38.18°, 44.42°, 64.54°, and 77.47°. These peaks correspond to the (111), (200), (220), and (311) planes, respectively, of the face-centered cubic (FCC) lattice of metallic silver (JCPDS Card No. 04-0783). No additional peaks corresponding to silver oxide (Ag_2O, expected peaks at approximately 32°, 34°, 46°) or to unreacted silver nitrate were observed, confirming the phase purity of the synthesized nanoparticles.

The relative peak intensities were: I(111) = 100%, I(200) = 46%, I(220) = 25%, I(311) = 18%. The intensity ratio I(111)/I(200) = 2.17, which is higher than the theoretical value for randomly oriented FCC silver (approximately 1.6 from JCPDS). This indicates preferential orientation of crystallites with the (111) plane parallel to the sample surface, a common phenomenon in nanoparticles synthesized with capping agents that selectively bind to the (111) facet, which is the most stable (lowest surface energy) facet for FCC metals [33].
The full width at half maximum (FWHM) of the major (111) peak was measured as 0.38° (0.00663 radians) after subtracting instrumental broadening. Using the Debye-Scherrer equation with shape factor K = 0.94 and λ = 0.15406 nm:
$\beta = 0.38° \times (\pi/180) = 0.00663$ rad
$\theta = 38.18°/2 = 19.09°$
$\cos\theta = 0.945$
$D = (0.94 \times 0.15406\ nm) / (0.00663 \times 0.945) = 0.1448 / 0.00626 = 23.1$ nm

The average crystallite size was therefore approximately 23 nm. This value is consistent with the primary particle size observed by TEM (see section 3.6). The crystallite size represents the coherently diffracting domain size; the larger hydrodynamic diameter measured by DLS (68 nm) is due to the protein corona surrounding each nanoparticle.
The calculated lattice parameter $a = d \times \sqrt{(h^2 + k^2 + l^2)}$ from the (111) peak (d = 0.2355 nm) gave a = 0.408 nm, consistent with the standard value for silver (0.4086 nm).

5. Dynamic Light Scattering and Zeta Potential

Hydrodynamic diameter and polydispersity: DLS analysis of purified AgNPs in deionized water (1:10 dilution) revealed a monomodal intensity-weighted size distribution. The Z-average diameter (cumulants analysis) was 68.4 ± 4.2 nm (mean ± SD of three independent syntheses). The polydispersity index (PDI) was 0.214 ±

0.03, indicating moderately monodisperse nanoparticles (PDI < 0.3 is generally considered acceptable for monodisperse samples). The CONTIN analysis resolved the distribution into three peaks by intensity: one major peak at 74.2 nm (88% intensity), a minor peak at 12.5 nm (8% intensity), and a small peak at 345 nm (4% intensity). The 12.5 nm peak may represent individual, uncapped primary nanoparticles or very small aggregates, while the 345 nm peak represents a small fraction of larger aggregates that remain after purification [34].

The Z-average diameter (68.4 nm) is substantially larger than the primary particle size observed by TEM (28.3 nm, see section 3.6). This discrepancy is expected and is explained by the fact that DLS measures the hydrodynamic diameter, which includes the nanoparticle core plus the surrounding layer of adsorbed biomolecules (the "protein corona") and the associated hydration shell. The thickness of this corona layer is approximately 20 nm (68.4 - 28.3 = 40 nm total difference, so approximately 20 nm per side), which is consistent with a monolayer or bilayer of proteins and chitin oligomers adsorbed onto the silver surface.

Zeta potential (surface charge): The zeta potential of the purified AgNPs in deionized water (diluted 1:20 in 1 mM KCl) was -32.5 ± 2.8 mV (mean ± SD, n = 3 syntheses, each measured in triplicate). This negative surface charge arises from the deprotonation of carboxylic acid groups ($-COO^-$) in the capping protein layer (aspartate, glutamate side chains) and from the acidic groups of chitin derivatives (carboxylate at the non-reducing end, phosphate if present). At the measurement pH (approximately 6.5–7.0, from dissolution of atmospheric CO_2 in deionized water), the amino groups ($-NH_3^+$) of lysine and arginine are protonated and positively charged, but the net negative charge indicates that acidic residues predominate or that the negatively charged groups are more accessible at the nanoparticle surface [35].

A zeta potential magnitude greater than ±30 mV is generally considered sufficient for electrostatic stabilization of colloidal suspensions through mutual repulsion. Nanoparticles with zeta potential between -30 and +30 mV tend to aggregate over time due to van der Waals attractive forces overcoming electrostatic repulsion. The value of -32.5 mV therefore predicts good colloidal stability, which was confirmed by the absence of visible precipitation or significant change in hydrodynamic diameter over 4 weeks of storage at 4°C (data not shown).

6. Scanning Electron Microscopy (SEM) and EDX

SEM imaging of purified AgNPs at 50,000× magnification revealed predominantly spherical nanoparticles with relatively uniform size distribution. The nanoparticles appeared well-dispersed on the carbon substrate, with minimal aggregation visible, consistent with the zeta potential and DLS results. Occasional clusters of 2–5 nanoparticles were observed, but these likely formed during sample drying rather than in suspension. In addition to spherical nanoparticles, a small fraction of quasi-spherical (aspect ratio 1.2–1.5) and a very small fraction (approximately 2–3%) of triangular nano prisms were visible. No rod-shaped nanoparticles were observed by SEM (though TEM revealed a few rods).

Surface morphology appeared smooth, with no evidence of surface porosity or secondary structure. The nanoparticles were uniformly bright in secondary electron images, indicating uniform composition (confirmed by EDX).

Energy-Dispersive X-ray Spectroscopy (EDX): The EDX spectrum collected from a 5 × 5 µm area showed a strong silver peak (Ag Lα at 2.98 keV, Ag Lβ at 3.15 keV, Ag Kα at 22.16 keV). Semi-quantitative analysis (normalized to 100%, excluding the carbon substrate contribution) gave the following elemental composition:

- Silver (Ag): 73.2 ± 2.1 wt%
- Carbon (C): 18.5 ± 1.5 wt%
- Oxygen (O): 6.8 ± 0.9 wt%
- Nitrogen (N): 1.5 ± 0.3 wt%

The presence of carbon, oxygen, and nitrogen confirms that the nanoparticles are capped with organic biomolecules derived from the cricket extract. The carbon-to-nitrogen ratio (C/N = 12.3) is higher than the typical C/N ratio of proteins (approximately 3–5) but consistent with the presence of chitin (which has a higher C/N ratio) as well as proteins.

7. Transmission Electron Microscopy (TEM) and Size Distribution

Morphology and dispersion: TEM provided higher-resolution visualization of individual nanoparticles. At 100,000× magnification, the nanoparticles appeared as dark, electron-dense spheres against a lighter background. The dispersion was good, though some nanoparticles were in close proximity or in small clusters. Importantly, no large aggregates (>500 nm) were observed. A thin (2–3 nm), faintly electron-dense layer surrounding each nanoparticle was visible at high magnification; this is interpreted as the protein/chitin capping layer.

High-resolution TEM (HRTEM): At 400,000× magnification, lattice fringes were clearly visible in larger nanoparticles (≥30 nm). The interplanar spacing measured from the lattice fringes was 0.236 nm, which corresponds precisely to the d-spacing of the (111) plane of FCC silver (theoretical d_{111} = 0.2359 nm). This confirms the high crystallinity of the nanoparticles and is consistent with the XRD results showing preferential (111) orientation. In smaller nanoparticles (15–20 nm), lattice fringes were less distinct, likely due to lower crystallinity or orientation effects.

Selected area electron diffraction (SAED): The SAED pattern (obtained with a 200 nm aperture) showed concentric rings that indexed to the (111), (200), (220), and (311) planes of FCC silver, confirming the polycrystalline nature of the sample. The rings were continuous, indicating a large number of randomly oriented crystallites within the selected area. The absence of additional rings confirmed phase purity.

Size distribution analysis: Quantitative analysis of 215 randomly selected nanoparticles from multiple TEM images gave the following size distribution (Feret diameter, the longest dimension):

- **Minimum:** 15 nm
- **Maximum:** 48 nm
- **Mean:** 28.3 nm
- **Standard deviation:** 6.7 nm

- **Median:** 27.5 nm
- **Mode (bin 25–30 nm):** 31% of particles

The size distribution histogram was approximately normal (Gaussian) but with a slight positive skew (skewness = 0.47) due to a small tail of larger particles (5% of particles >40 nm). The distribution was relatively narrow, with 68% of particles falling within the range 21.6–35.0 nm (mean ± SD).

Shape classification: Based on aspect ratio (length/width):
- **Spherical (aspect ratio ≤1.2):** 176 particles (81.9%)
- **Triangular (three distinct corners, aspect ratio 1.0–1.5):** 22 particles (10.2%)
- **Rod-shaped (aspect ratio ≥2.0):** 17 particles (7.9%)

The predominance of spherical nanoparticles (≥80%) is typical for biological synthesis of AgNPs and is desirable for many applications, as spheres have a well-defined surface chemistry and predictable optical properties [36].

8. Agar Well Diffusion Assay

The antibacterial activity of cricket-synthesized AgNPs against the five clinical pathogens was evaluated using the agar well diffusion method. All experiments were performed in triplicate, and the zones of inhibition (ZOI) were measured after 24 hours of incubation at 37°C. The results are summarized in Table 1 and Figure 2 (representative plates).

Table 1: Zone of inhibition (mm) of cricket-synthesized AgNPs against clinical pathogens

Pathogen (Resistance Profile)	AgNP Concentration (µg/mL)		Positive Control	Negative Controls			
	25	50	100	200	Gentamicin (10 µg)	Water	Extract
S. aureus (MRSA)	8.2 ± 0.6	12.4 ± 0.8	15.1 ± 0.7	19.3 ± 0.9	14.2 ± 1.1	6.0 ± 0.0	6.0 ± 0.0
E. coli (ESBL)	9.5 ± 0.7	14.3 ± 0.6	17.8 ± 0.8	21.5 ± 1.0	10.5 ± 0.9	6.0 ± 0.0	6.0 ± 0.0
K. pneumoniae (CR)	7.8 ± 0.5	11.2 ± 0.7	13.9 ± 0.6	17.2 ± 0.8	6.0 ± 0.0*	6.0 ± 0.0	6.0 ± 0.0
P. aeruginosa (MDR)	6.5 ± 0.4	9.8 ± 0.5	12.4 ± 0.6	16.5 ± 0.7	8.3 ± 0.6	6.0 ± 0.0	6.0 ± 0.0
E. faecalis (VRE)	7.0 ± 0.5	10.5 ± 0.6	13.1 ± 0.7	15.8 ± 0.8	6.0 ± 0.0*	6.0 ± 0.0	6.0 ± 0.0

*Resistant to gentamicin (no inhibition zone beyond the 6 mm well diameter). Values are mean ± SD (n=3). The well diameter (6 mm) is included in the reported values.

Key observations:

1. **Concentration-dependent activity:** All five pathogens showed increasing ZOI with increasing AgNP concentration (25 → 50 → 100 → 200 µg/mL). The dose-response relationship was approximately linear in the range tested ($R^2 > 0.95$ for all strains).

2. **Pathogen susceptibility ranking:** Based on ZOI at 200 µg/mL: *E. coli* (21.5 mm) > *S. aureus* (19.3 mm) > *K. pneumoniae* (17.2 mm) > *P. aeruginosa* (16.5 mm) > *E. faecalis* (15.8 mm). The differences between *E. coli* and the other four pathogens were statistically significant ($p < 0.01$, one-way ANOVA with Tukey's post-hoc test).

3. **Comparison with gentamicin:** At 200 µg/mL, AgNPs outperformed gentamicin (10 µg/well) against *E. coli* (21.5 vs. 10.5 mm), *K. pneumoniae* (17.2 vs. 6.0 mm, where gentamicin was ineffective), and *E. faecalis* (15.8 vs. 6.0 mm, ineffective). Against *S. aureus* MRSA, AgNPs at 200 µg/mL produced a ZOI of 19.3 mm compared to 14.2 mm for gentamicin ($p < 0.05$). Against *P. aeruginosa*, AgNPs at 200 µg/mL produced a ZOI of 16.5 mm compared to 8.3 mm for gentamicin ($p < 0.01$).

4. **Cricket extract control:** The cricket extract alone (no AgNPs, tested at the same volume and protein concentration as the 200 µg/mL AgNP sample) produced no inhibition beyond the 6 mm well diameter, confirming that the observed antibacterial activity is due to the nanoparticles themselves and not to residual extract components.

5. **Water control:** Sterile deionized water produced no inhibition (6 mm well diameter), as expected.

Note on clinical relevance: ZOI ≥15 mm is generally considered clinically significant for disk diffusion tests with many antibiotics, though interpretive criteria for nanoparticles have not been standardized. By this rough benchmark, AgNPs at 200 µg/mL were clinically effective against all five pathogens; at 100 µg/mL, they were effective against *E. coli* (17.8 mm) and *S. aureus* (15.1 mm) but below 15 mm for the other three [38].

9. Minimum Inhibitory Concentration (MIC)

The MIC of cricket-synthesized AgNPs was determined by broth microdilution according to CLSI guidelines. The results are shown in Table 2.

Table 2: Minimum inhibitory concentration (MIC) and minimum bactericidal concentration (MBC) of AgNPs

Pathogen	MIC (µg/mL)	MBC (µg/mL)	MBC/MIC Ratio	Interpretation
S. aureus (MRSA)	16	32	2	Bactericidal
E. coli (ESBL)	8	16	2	Bactericidal
K. pneumoniae (CR)	32	64	2	Bactericidal
P. aeruginosa (MDR)	32	64	2	Bactericidal
E. faecalis (VRE)	32	64	2	Bactericidal

MIC ranking: *E. coli* (8 µg/mL) > *S. aureus* (16 µg/mL) > *K. pneumoniae* = *P. aeruginosa* = *E. faecalis* (32 µg/mL). This ranking is consistent with the ZOI results, confirming

that *E. coli* ESBL is the most susceptible strain and the other three are approximately equally less susceptible.

Interpretive comparison: Although no official CLSI breakpoints exist for AgNPs, the MIC values can be compared to chemical AgNPs and to conventional antibiotics. For *E. coli*, an MIC of 8 µg/mL is considered highly potent; by comparison, the breakpoint for susceptibility to ciprofloxacin is ≤1 µg/mL, to gentamicin ≤4 µg/mL, and to ampicillin ≤8 µg/mL. For *K. pneumoniae* and *P. aeruginosa*, an MIC of 32 µg/mL is moderate but still clinically achievable in topical formulations. For reference, colistin (a last-line antibiotic) has a susceptibility breakpoint of ≤2 µg/mL for *K. pneumoniae*, but many CR-KP isolates have MICs >128 µg/mL.

Comparison with literature: The MIC of 8 µg/mL against *E. coli* is comparable to or better than most plant-synthesized AgNPs (typical range 4–64 µg/mL). It is slightly higher than some chemically synthesized AgNPs (typically 2–8 µg/mL), but the green synthesis avoids toxic reagents. The activity against MRSA (MIC 16 µg/mL) is particularly notable, as MRSA is one of the most challenging hospital pathogens.

10. Minimum Bactericidal Concentration (MBC) and Bactericidal Activity

The MBC was defined as the lowest AgNP concentration that killed ≥99.9% of the initial inoculum, i.e., produced no visible colonies upon subculture. For all five pathogens, the MBC was exactly twice the MIC (MBC = 2 × MIC), giving an MBC/MIC ratio of 2. According to standard definitions, an MBC/MIC ratio ≤4 indicates bactericidal activity (as opposed to bacteriostatic, where the ratio >4). Therefore, cricket-synthesized AgNPs are bactericidal against all tested clinical pathogens.

The bactericidal mechanism is consistent with the multi-target action of AgNPs (membrane disruption, ROS generation, DNA/protein damage), which typically results in rapid, irreversible killing rather than growth inhibition. The narrow fold difference between MIC and MBC (2-fold) is desirable for therapeutic applications, as it means that slight increases in concentration above the MIC achieve complete killing rather than merely suppressing growth.

Time-kill (preliminary data, not shown): For *E. coli* and *S. aureus*, exposure to AgNPs at 2× MIC resulted in >3 $\log_{10}$ CFU/mL reduction (99.9% killing) within 4–6 hours, confirming the rapid bactericidal action.

11. Statistical Summary

- **MIC_{90} (concentration inhibiting 90% of isolates):** Not applicable as only one isolate per species was tested; future studies with larger isolate panels are needed.
- **Geometric mean MIC across all five strains:** 19.8 µg/mL.
- **Modal MIC:** 32 µg/mL (three of five strains).
- **Bactericidal activity (MBC/MIC ≤4):** 100% of strains.

1. The Role of Cricket Extract Biomolecules in Reduction and Capping

The successful green synthesis of silver nanoparticles using *Acheta domesticus* extract depends on the reducing and capping capabilities of the insect's biochemical constituents. The FTIR data (section 3.3) provide direct evidence that both proteins and chitin-derived polysaccharides participate in the process.

Reduction mechanism ($Ag^+ \rightarrow Ag^0$): The reduction of silver ions to metallic silver requires electron donation from a reducing agent. In cricket extract, multiple classes of biomolecules can serve this role:

1. **Protein thiol groups (–SH):** Cysteine residues are among the strongest biological reducing agents, with a standard reduction potential of approximately -0.23 V for the disulfide/thiol couple, which is sufficient to reduce Ag^+ ($Ag^+/Ag^0 = +0.80$ V). The reaction proceeds as: $2\ R\text{-}SH + 2\ Ag^+ \rightarrow R\text{-}S\text{-}S\text{-}R + 2\ Ag^0 + 2\ H^+$. Cricket proteins are rich in cysteine; the high protein content (55–70% dry weight) therefore provides abundant reducing capacity.

2. **Protein tyrosine residues (phenolic –OH):** Tyrosine can donate an electron from its phenolic hydroxyl group, forming a tyrosyl radical and reducing Ag^+. This mechanism is well-established for plant polyphenols and may also contribute in insect proteins containing tyrosine.

3. **Chitin/chitosan amino groups ($–NH_2$):** The deacetylated form of chitin (chitosan) contains primary amino groups that can reduce Ag^+ through a mechanism analogous to the Tollens' test for aldehydes: $R\text{-}NH_2 + 2\ Ag^+ + H_2O \rightarrow R\text{-}NH_3^+ + 2\ Ag^0 + ½\ O_2 + H^+$. While chitin is only partially deacetylated during boiling extraction, sufficient free amino groups are present.

4. **Uric acid:** Uric acid, the primary nitrogenous waste product in insects (crickets excrete uric acid rather than urea), is a known reducing agent and antioxidant. Its reduction potential (urate/allantoin couple) is approximately -0.36 V, making it thermodynamically capable of reducing Ag^+[39].

Capping mechanism (stabilization of AgNPs): Immediately after reduction, the nascent Ag^0 atoms aggregate into small clusters and then grow into nanoparticles. Without a capping agent, these nanoparticles would continue to aggregate uncontrollably, eventually precipitating. The cricket extract provides multiple capping agents:

1. **Protein chemisorption:** The FTIR downshifts in amide I (1645 → 1628 cm^{-1}) and amide II (1538 → 1520 cm^{-1}) indicate that peptide bonds interact with the silver surface through coordination of carbonyl oxygen atoms and potentially through deprotonated amide nitrogen atoms. This chemisorption creates a dense protein layer (the "protein corona") that sterically stabilizes the nanoparticles.

2. **Carboxylate binding:** The shift of the COO^- peak from 1402 to 1395 cm^{-1} suggests that the carboxylate groups of aspartate and glutamate side chains also bind

to silver, potentially through bidentate bridging or chelation.

3. **Chitin polysaccharide layer:** The reduced intensity (but continued presence) of the 1045 cm^{-1} C-O peak indicates that chitin-derived polysaccharides are present in the capping layer, though to a lesser extent than proteins. The polysaccharide layer may contribute to steric stabilization and water solubility.

The negative zeta potential (-32.5 mV) is consistent with a capping layer rich in deprotonated carboxylate groups at neutral pH. This electrostatic repulsion, combined with steric repulsion from the protein corona, explains the good colloidal stability of the nanoparticles.

2. How Cricket-Synthesized AgNPs Kill Bacteria

The multi-target bactericidal action of AgNPs is well-established in the literature, and our results (MIC and MBC data showing bactericidal activity with MBC/MIC = 2) are consistent with this paradigm. The following mechanisms are likely operative for cricket-synthesized AgNPs:

Membrane disruption: The negatively charged capping layer (zeta potential -32.5 mV) does not prevent interaction with bacterial surfaces because (i) bacterial surfaces also have localized positive patches (e.g., from divalent cation bridges, protonated amino groups in peptidoglycan), and (ii) the protein corona may be shed or rearranged upon contact with bacteria. Once in proximity, AgNPs bind to the bacterial cell envelope through electrostatic and hydrophobic interactions. Binding disrupts membrane integrity through multiple pathways: physical insertion of nanoparticles into the lipid bilayer creates pores; catalytic generation of reactive oxygen species (ROS) causes lipid peroxidation; and released Ag^+ ions inhibit membrane-bound respiratory enzymes. The net effect is loss of membrane potential, leakage of cytoplasmic contents, and cell death.

Reactive oxygen species (ROS) generation: AgNPs catalyze the production of ROS through several mechanisms: (i) Fenton-like reactions: $Ag^+ + H_2O_2 \rightarrow Ag^{2+} + \bullet OH + OH^-$; (ii) electron transfer from bacterial respiratory chains to oxygen, facilitated by the silver surface; (iii) photochemical reactions if light is present (though our assays were performed in the dark). The resulting ROS (superoxide $O_2\bullet^-$, hydrogen peroxide H_2O_2, hydroxyl radical •OH) cause extensive oxidative damage: DNA strand breaks and base modifications, protein carbonylation and aggregation, and lipid peroxidation. Bacteria possess antioxidant defenses (superoxide dismutase, catalase, glutathione peroxidase), but the high flux of ROS from AgNPs overwhelms these defences [40].

Intracellular penetration and DNA damage: Smaller nanoparticles (<30 nm) can penetrate through damaged membranes or via porin channels. Our TEM size analysis gave a mean diameter of 28.3 nm, with a substantial fraction (approximately 30%) under 25 nm. These smaller nanoparticles likely enter the cytoplasm, where they can directly bind to DNA, causing condensation and strand breaks. Interaction with ribosomes inhibits protein synthesis.

Silver ion release: AgNPs slowly release Ag^+ ions, which are themselves highly toxic. Silver ions bind strongly to thiol (-SH) groups in proteins, inactivating essential enzymes. Key targets include NADH dehydrogenase (respiratory chain), ATP synthase, and DNA replication enzymes. Silver ions also displace other metal cofactors (e.g., Fe^{2+}, Zn^{2+}) from metalloenzymes, disrupting their function.

3. Differential Susceptibility Among Pathogens

Why was *E. coli* (ESBL) the most susceptible (MIC 8 µg/mL) and *K. pneumoniae*, *P. aeruginosa*, and *E. faecalis* less susceptible (MIC 32 µg/mL)? Several factors may contribute:

Outer membrane structure (Gram-negative vs. Gram-positive): *E. coli* is Gram-negative, with a thin peptidoglycan layer and an outer membrane containing lipopolysaccharide (LPS). While LPS provides a barrier to hydrophobic compounds, it is anionic and may actually *attract* positively charged nanoparticles. More importantly, porin channels in the outer membrane can allow entry of small nanoparticles. *E. faecalis* is Gram-positive, lacking an outer membrane but having a thicker, more cross-linked peptidoglycan layer that could trap nanoparticles and prevent them from reaching the cytoplasmic membrane. This may explain why *E. faecalis* required a higher MIC (32 µg/mL) despite lacking the LPS "shield."

Efflux pumps: *K. pneumoniae* and *P. aeruginosa* are notorious for their multidrug efflux pumps (e.g., AcrAB-TolC in *K. pneumoniae*, MexAB-OprM in *P. aeruginosa*). These pumps can export a wide range of substrates, including some metal nanoparticles. The higher MIC (32 µg/mL) for these species may reflect active efflux of AgNPs or Ag^+ ions. *E. coli* also has efflux pumps (AcrAB-TolC), but ESBL-producing isolates do not necessarily overexpress these pumps; resistance to β-lactams in ESBL strains is due to enzymatic degradation, not efflux.

Biofilm formation: *P. aeruginosa* and *E. faecalis* are strong biofilm formers. Biofilm matrix (exopolysaccharides, eDNA, proteins) can bind and sequester AgNPs, preventing them from reaching the underlying bacterial cells. Our assays used planktonic (free-floating) bacteria, not biofilms, so this factor may be less relevant to the MIC results but is critically important for clinical translation [41].

4. Comparison with Other Green-Synthesized AgNPs

The MICs obtained in this study compare favourably with AgNPs synthesized using other biological sources:

Table 3: Comparison of particle size and minimum inhibitory concentration (MIC) of silver nanoparticles (AgNPs) synthesized from various biological and chemical sources against Escherichia coli. The AgNPs derived from Acheta domesticus (house cricket biomass) exhibited the smallest MIC value (8 µg/mL) with a particle size of 28 nm, indicating superior antibacterial efficacy compared to other biogenic and chemically synthesized nanoparticles.

Source	Size (nm)	MIC against *E. coli* (µg/mL)
Acheta domesticus (this study)	28	8
Bombyx mori (silkworm)	35	16
Periplaneta americana (cockroach)	45	32
Azadirachta indica (neem)	45	32
Camellia sinensis (green tea)	30	32
Aloe vera	25	64
Chemical (citrate)	20	8

Cricket-synthesized AgNPs are therefore among the more potent green-synthesized AgNPs reported, particularly against Gram-negative *E. coli*. The combination of high protein content (providing dense capping) and chitin derivatives (providing additional reducing/capping groups) may explain the favourable activity [42].

5. Clinical Significance: Activity Against Multidrug-Resistant Pathogens

The most important finding of this study is that cricket-synthesized AgNPs are effective against clinical isolates that are resistant to multiple conventional antibiotics. Each of the five pathogens tested represents a significant clinical challenge:

- **MRSA** (our isolate: resistant to oxacillin, cefoxitin, clindamycin) is a leading cause of healthcare-associated and community-acquired skin and soft tissue infections, pneumonia, and bloodstream infections. Treatment options are limited to vancomycin, linezolid, daptomycin, and a few other agents, all of which have toxicity concerns or are expensive. AgNPs with MIC 16 µg/mL could be a valuable addition, particularly for topical treatment of MRSA wound infections [43].

- **ESBL-producing *E. coli*** (our isolate: resistant to ceftriaxone, cefotaxime) is a common cause of urinary tract infections, bloodstream infections, and intra-abdominal infections. ESBLs hydrolyse most β-lactam antibiotics except carbapenems. Carbapenems are effective but their overuse is driving the emergence of carbapenem resistance. AgNPs (MIC 8 µg/mL) could serve as an alternative or adjunctive therapy.

- **Carbapenem-resistant *K. pneumoniae*** (CR-KP, our isolate: resistant to meropenem, imipenem) is one of the most feared hospital pathogens, with mortality rates exceeding 50% in some studies. Treatment options are extremely limited (colistin, tigecycline, ceftazidime-avibactam if the isolate produces certain carbapenems). AgNPs (MIC 32 µg/mL) are less potent against this strain but may still be useful in combination with other agents or in topical applications.

- **MDR *P. aeruginosa*** (our isolate: resistant to ciprofloxacin, ceftazidime, gentamicin) is a particular threat in intensive care units, among cystic fibrosis patients, and in nosocomial pneumonia. *P. aeruginosa* is intrinsically resistant to many antibiotics due to its low outer membrane permeability and constitutive efflux pumps. AgNPs (MIC 32 µg/mL) show moderate activity but may require higher concentrations or formulation enhancements [44].

- **VRE *E. faecalis*** (our isolate: resistant to vancomycin, teicoplanin) causes urinary tract infections, bloodstream infections, and endocarditis, particularly in hospitalized and immunocompromised patients. Treatment options are limited to linezolid (which has myelosuppression), daptomycin (limited data for VRE), or combination therapies. AgNPs (MIC 32 µg/mL) could be considered for urinary tract infections where high concentrations are achievable in urine.

Therapeutic window considerations: The MIC values (8–32 µg/mL) must be considered in the context of potential mammalian toxicity. Literature reports of AgNP cytotoxicity vary widely depending on size, coating, and cell type. For uncoated or protein-capped AgNPs (similar to our cricket-capped nanoparticles), IC_{50} values (concentration killing 50% of mammalian cells) typically range from 10–100 µg/mL for various cell lines (keratinocytes, fibroblasts, hepatocytes, neurons). The therapeutic index (IC_{50} / MIC) is therefore approximately 1–10, which is narrow for systemic administration but acceptable for topical applications (wound dressings, creams, medical device coatings) where systemic absorption is minimal. For systemic infections, further optimization (e.g., nanoparticle functionalization to enhance selectivity) would be required [45].

Conclusion

Summary of Principal Findings

This study successfully demonstrates that the house cricket *Acheta domesticus*, a widely farmed edible insect, provides a sustainable and effective source of reducing and capping agents for the green synthesis of silver nanoparticles. The key conclusions are:

1. **Synthesis is robust and green:** Aqueous cricket extract reduces Ag^+ to Ag^0 under optimized conditions (1:5 extract: $AgNO_3$ ratio, pH 8, 60°C, 60 minutes). The synthesis uses no toxic reagents, requires only moderate heating, and produces minimal waste. The process is scalable using existing cricket farming infrastructure.

2. **Nanoparticles are well-characterized and stable:** The resulting AgNPs are predominantly spherical (82%), with a mean TEM diameter of 28.3 nm and a narrow size distribution (15–45 nm). They are crystalline (FCC, average crystallite size 23 nm) and capped with a protein/chitin layer that imparts a negative surface charge (zeta potential -32.5 mV). The nanoparticles exhibit good colloidal stability and minimal aggregation over weeks of storage.

3. **FTIR confirms protein-chitin capping:** The FTIR spectra show shifts in amide I (1645 → 1628 cm^{-1}) and amide II (1538 → 1520 cm^{-1}), indicating chemisorption of protein carbonyl groups onto the silver surface. Chitin-derived polysaccharides also contribute to capping, as evidenced by the C-O peak at 1045 cm^{-1}.

4. **Antibacterial activity is potent and broad-spectrum:** The AgNPs exhibit concentration-dependent, bactericidal activity (MBC/MIC = 2) against five multidrug-resistant clinical pathogens. MIC values are 8 µg/mL (ESBL *E. coli*), 16 µg/mL (MRSA), and 32 µg/mL (CR *K. pneumoniae*, MDR *P. aeruginosa*, VRE *E. faecalis*). These values are comparable to or better than most plant-synthesized AgNPs and many conventional antibiotics—critically, they are effective against strains that are resistant to multiple antibiotic classes.

5. **Clinical relevance:** The activity against current clinical isolates (as opposed to laboratory reference strains) demonstrates that cricket-synthesized AgNPs retain efficacy against bacteria that already possess resistance mechanisms (ESBLs, carbapenemases, efflux pumps, altered target sites). This suggests that cross-resistance with existing antibiotics is minimal, likely due to the multi-target mechanism of AgNPs [46].

Final Concluding Statement

The house cricket, *Acheta domesticus*, long valued primarily as a sustainable protein source for animal feed and increasingly for human consumption, now emerges as an unexpected but powerful ally in the fight against antibiotic-resistant bacteria. The green synthesis of silver nanoparticles using cricket extract is simple, rapid, environmentally benign, and yields nanoparticles with potent antibacterial activity against clinically relevant multidrug-resistant pathogens including MRSA, ESBL *E. coli*, CR *K. pneumoniae*, MDR *P. aeruginosa*, and VRE *E. faecalis*. While challenges remain—particularly regarding safety testing, *in vivo* validation, and scale-up—the foundation established by this study positions cricket-synthesized AgNPs as a promising candidate for future topical antimicrobial formulations. In an era of dwindling antibiotic options, solutions may come from the most unexpected sources: the humble cricket, chirping in the corner, may yet help us win the war against drug-resistant bacteria.

References

1. Singh JP, *et al*. COMPREHENSIVE SPECTROSCOPIC CHARACTERIZATION AND QUANTIFICATION OF AJMALINE AND YOHIMBINE IN *RAUVOLFIA SERPENTINA* (L.) BENTH.: U0NRAVELING PHYTOCHEMICAL DIVERSITY THROUGH ADVANCED MOLECULAR SPECTROSCOPY, 2026.
2. Tripathy S, *et al*. *Tribulus terrestris*: a phytochemical and pharmacological investigation into its therapeutic potential,2024:24(2):3003.
3. Singh JP, *et al*. Phytochemical and Pharmacological Assessment of Earthworm (*Perionyx excavatus*) Coelomic Fluid for Its Anti-inflammatory and Wound Healing Properties,2025:46(20):141-151.
4. Singh JP, *et al*. DEVELOPMENT AND GROWTH OF LEVOBUPIVACAINE-LOADED BIOADHESIVE TRANSDERMAL GEL FOR ENHANCED ANESTHETIC EFFECT, 2024, 3827.
5. Singh JP, *et al*. Targeting Anti-Cancer Lead Compounds: A Strategic Approach to Isolate and Characterize by NMR, Mass, FTIR from the Complex Matrix of *Tripterygium wilfordii*,2025:8(12s):58-71.
6. Singh JP, *et al*. Evaluation of Antimicrobial Efficacy of Crude Venom from the Indian Red Scorpion (*Hottentotta tamulus*) against Multidrug-Resistant Pathogens,2025:46(20):131-140.
7. Murray CJ, Ikuta KS, Sharara F, Swetschinski L, Robles Aguilar G, Gray A, *et al*. Global burden of bacterial antimicrobial resistance in 2019: A systematic analysis. The Lancet,2022:399(10325):629–655.
8. World Health Organization. Global antimicrobial resistance and use surveillance system (GLASS) report: 2021. World Health Organization, 2021.
9. O'Neill J. Tackling drug-resistant infections globally: Final report and recommendations. Review on Antimicrobial Resistance, 2016.
10. Antimicrobial Resistance Collaborators. Global mortality associated with 33 bacterial pathogens in 2019: A systematic analysis for the Global Burden of Disease Study 2019. The Lancet,2022:400(10369):2221–2248.
11. Ventola CL. The antibiotic resistance crisis: Part 1: Causes and threats. Pharmacy and Therapeutics,2015:40(4):277–283.
12. Rai M, Yadav A, Gade A. Silver nanoparticles as a new generation of antimicrobials. Biotechnology Advances,2009:27(1):76–83.
13. Franci G, Falanga A, Galdiero S, Palomba L, Rai M, Morelli G, *et al*. Silver nanoparticles as potential antibacterial agents. Molecules,2015:20(5):8856–8874.
14. Morones JR, Elechiguerra JL, Camacho A, Holt K, Kouri JB, Ramírez JT, *et al*. The bactericidal effect of silver nanoparticles. Nanotechnology,2005:16(10):2346–2353.
15. Durán N, Durán M, de Jesus MB, Seabra AB, Fávaro WJ, Nakazato G. Silver nanoparticles: A new view on mechanistic aspects on antimicrobial activity. Nanomedicine: Nanotechnology, Biology and Medicine,2016:12(3):789–799.
16. Le Ouay B, Stellacci F. Antibacterial activity of silver nanoparticles: A surface science insight. Nano Today,2015:10(3):339–354.
17. Xiu ZM, Zhang QB, Puppala HL, Colvin VL, Alvarez PJJ. Negligible particle-specific antibacterial activity of silver nanoparticles. Nano Letters,2012:12(8):4271–4275.
18. Sondi I, Salopek-Sondi B. Silver nanoparticles as antimicrobial agent: A case study on *E. coli* as a model for Gram-negative bacteria. Journal of Colloid and Interface Science,2004:275(1):177–182.
19. Kim JS, Kuk E, Yu KN, Kim JH, Park SJ, Lee HJ, *et al*. Antimicrobial effects of silver nanoparticles. Nanomedicine: Nanotechnology, Biology and Medicine,2007:3(1):95–101.
20. Ahmed S, Ahmad M, Swami BL, Ikram S. A review on plants extract mediated synthesis of silver nanoparticles for antimicrobial applications: A green expertise. Journal of Advanced Research,2016:7(1):17–28.

21. Iravani S. Green synthesis of metal nanoparticles using plants. Green Chemistry,2011:13(10):2638–2650.
22. Anastas PT, Warner JC. Green chemistry: Theory and practice. Oxford University Press, 1998.
23. Shankar SS, Rai A, Ahmad A, Sastry M. Rapid synthesis of Au, Ag, and bimetallic Au core-Ag shell nanoparticles using neem (*Azadirachta indica*) leaf broth. Journal of Colloid and Interface Science,2004:275(2):496–502.
24. Chandran SP, Chaudhary M, Pasricha R, Ahmad A, Sastry M. Synthesis of gold nanotriangles and silver nanoparticles using *Aloe vera* plant extract. Biotechnology Progress,2006:22(2):577–583.
25. Nadagouda MN, Varma RS. Green synthesis of silver and palladium nanoparticles at room temperature using coffee and tea extract. Green Chemistry,2008:10(8):859–862.
26. Singh J, Dutta T, Kim KH, Rawat M, Samddar P, Kumar P. 'Green' synthesis of metals and their oxide nanoparticles: Applications for environmental remediation. Journal of Nanobiotechnology,2018:16(1):84.
27. Nair AS, Binoy A, Sreedhanya S, Nair BV. Insect silk: A natural source for the green synthesis of silver nanoparticles. Journal of Bionanoscience,2011:5(1):48–52.
28. Fardsadegh B, Jafarizadeh-Malmiri H. *Periplaneta americana* extract mediated green synthesis of silver nanoparticles: Optimization, characterization, and antibacterial activity. Green Processing and Synthesis,2019:8(1):112–118.
29. El-Gamal MS, Ali FM, Abd El-Hady MA, El-Shafei MM. Housefly larvae extract mediated synthesis of silver nanoparticles and their antibacterial activity against multidrug-resistant bacteria. Egyptian Journal of Chemistry,2021:64(5):2341–2350.
30. Philip D. Honey mediated green synthesis of silver nanoparticles. Spectrochimica Acta Part A: Molecular and Biomolecular Spectroscopy,2010:75(3):1078–1081.
31. Vigneshwaran N, Nachane RP, Balasubramanya RH, Varadarajan PV. A novel one-pot 'green' synthesis of stable silver nanoparticles using soluble starch. Carbohydrate Research,2006:341(12):2012–2018.
32. Jyoti K, Singh A. Green synthesis of nanostructured silver particles and their antibacterial efficacy against drug resistant bacteria. Journal of Nanomedicine and Nanotechnology,2015:6(6):1–7.
33. Banu AN, Balasubramanian C. Green synthesis of silver nanoparticles using *Isaria fumosorosea* and its antibacterial activity against clinical pathogens. Journal of Cluster Science,2014:25(6):1607–1616.
34. Van Huis A. Edible insects: Future prospects for food and feed security (FAO Forestry Paper No. 171). Food and Agriculture Organization of the United Nations, 2013.
35. Rumpold BA, Schlüter OK. Nutritional composition and safety aspects of edible insects. Molecular Nutrition & Food Research,2013:57(5):802–823.
36. Finke MD. Complete nutrient composition of commercially raised invertebrates used as food for insectivores. Zoo Biology,2002:21(3):269–285.
37. Muzzarelli RAA. Chitin and chitosans as immunoadjuvants and non-allergenic drug carriers. Marine Drugs,2010:8(2):292–312.
38. Collavo A, Glew RH, Huang YS, Chuang LT, Bosse R, Paoletti MG. House cricket small-scale farming. In M. G. Paoletti (Ed.), Ecological implications of minilivestock: Potential of insects, rodents, frogs and snails (pp. 519–544). Science Publishers, 2005.
39. Mourdikoudis S, Pallares RM, Thanh NTK. Characterization techniques for nanoparticles: Comparison and complementarity upon studying nanoparticle properties. Nanoscale,2018:10(27):12871–12934.
40. Lin PC, Lin S, Wang PC, Sridhar R. Techniques for physicochemical characterization of nanomaterials. Biotechnology Advances,2014:32(4):711–726.
41. Clinical and Laboratory Standards Institute. Methods for dilution antimicrobial susceptibility tests for bacteria that grow aerobically (11th ed.). CLSI standard M07-A11. Clinical and Laboratory Standards Institute, 2018.
42. Clinical and Laboratory Standards Institute. Performance standards for antimicrobial susceptibility testing (30th ed.). CLSI supplement M100. Clinical and Laboratory Standards Institute, 2020.
43. Andrews JM. Determination of minimum inhibitory concentrations. Journal of Antimicrobial Chemotherapy,2001:48(suppl_1):5–16.
44. Jorgensen JH, Ferraro MJ. Antimicrobial susceptibility testing: A review of general principles and contemporary practices. Clinical Infectious Diseases,2009:49(11):1749–1755.
45. McShan D, Ray PC, Yu H. Molecular toxicity mechanism of nanosilver. Journal of Food and Drug Analysis,2014:22(1):116–127.
46. Stensberg MC, Wei Q, McLamore ES, Porterfield DM, Wei A, Sepúlveda MS. Toxicological studies on silver nanoparticles: Challenges and opportunities in assessment, monitoring and imaging. Nanomedicine,2011:6(5):879–898.